

RESEARCH ARTICLE

STEM CELLS AND REGENERATION

Zebrafish midbrain slow-amplifying progenitors exhibit high levels of transcripts for nucleotide and ribosome biogenesis

Gaëlle Recher^{1,2,*}, Julia Jouralet^{1,3,*}, Alessandro Brombin^{1,3}, Aurélie Heuzé^{1,3}, Emilie Mugniery^{1,3}, Jean-Michel Hermel^{1,3}, Sophie Desnoullez^{1,2}, Thierry Savy^{1,2}, Philippe Herbomel^{4,5}, Franck Bourrat^{1,3}, Nadine Peyriéras^{1,2,§}, Françoise Jamen^{1,3,6,‡} and Jean-Stéphane Joly^{1,3,‡,§}

ABSTRACT

Investigating neural stem cell (NSC) behaviour *in vivo*, which is a major area of research, requires NSC models to be developed. We carried out a multilevel characterisation of the zebrafish embryo peripheral midbrain layer (PML) and identified a unique vertebrate progenitor population. Located dorsally in the transparent embryo midbrain, these large slow-amplifying progenitors (SAPs) are accessible for long-term *in vivo* imaging. They form a neuroepithelial layer adjacent to the optic tectum, which has transitory fast-amplifying progenitors (FAPs) at its margin. The presence of these SAPs and FAPs in separate domains provided the opportunity to data mine the ZFIN expression pattern database for SAP markers, which are co-expressed in the retina. Most of them are involved in nucleotide synthesis, or encode nucleolar and ribosomal proteins. A mutant for the *cad* gene, which is strongly expressed in the PML, reveals severe midbrain defects with massive apoptosis and sustained proliferation. We discuss how fish midbrain and retina progenitors might derive from ancient sister cell types and have specific features that are not shared with other SAPs.

KEY WORDS: Neural stem cell, Optic tectum, Retina

INTRODUCTION

In neural stem cells (NSCs) and neural progenitors (NPs), as in other cell types, cell identity is characterised by specific molecular signatures that depend on the environment provided by neighbouring cells (Fuchs et al., 2004). It is therefore important to study NPs *in vivo*. However, few *in vivo* investigations have been performed so far and these have mainly focused on two telencephalic populations in rodents: the subventricular zone (SVZ) and the dentate gyrus of the hippocampus (Zhao et al., 2008; Chojnacki et al., 2009; Kriegstein and Alvarez-Buylla, 2009; Hsieh, 2012). Teleosts and amphibians display an extraordinary capacity for NP activation and maintenance, but also for self-repair and neuronal regeneration in adulthood (Grandel et al., 2006; Zupanc, 2009; Kizil et al., 2011; Zupanc and Sîrbulescu, 2011; Schmidt et al., 2013). They are therefore excellent models for comparative

studies of the NP-based mechanisms underlying neural regeneration and are suitable for studies involving transgenesis and also for live imaging (Rieger et al., 2011; Rinkwitz et al., 2011).

One of the most interesting neurogenic areas, which has been described in both medaka (Alunni et al., 2010) and zebrafish (Grandel et al., 2006; Ito et al., 2010; Grandel and Brand, 2013), is located at the medial, lateral and caudal margins of the adult optic tectum (OT). The OT is a prominent dorsal region of the midbrain that functions as a cellular ‘conveyor belt’ (Devès and Bourrat, 2012). In this cortical structure there is a spatiotemporal correlation between the maturation state of a cell and its position in the OT. Each cell population, at a particular level of differentiation, is marked by concentric gene expression patterns. Similarly, the anamniote retina may be considered a cellular conveyor belt and, as discussed in a recent review (Cerveny et al., 2012), tectal cells and retina cells from the ciliary marginal zone (CMZ) share common molecular signatures and express many canonical proliferation markers.

Here we present an integrated study using zebrafish embryos to examine a population of label-retaining multipotent midbrain NPs. This population connects the OT to the torus semicircularis (TS) (a more ventral, but also an alar, midbrain structure) posteriorly and laterally. Medially, it also connects the OT to the cerebellum. Previously described as the ‘caudal wall’ (Palmgren, 1921) and recently as the ‘posterior midbrain lamina’ (Grandel et al., 2006), this structure wraps the embryonic OT both posteriorly and laterally; we therefore find it more appropriate to refer to this structure as the ‘peripheral midbrain layer’ (PML). Three recently published reviews (Cerveny et al., 2012; Grandel and Brand, 2013; Schmidt et al., 2013) pointed out the need to know more about the formation and function of this cell layer, which gives rise to different types of tectal cells. It is in close proximity with the *her5*-positive stem cells (SCs) at the midbrain-hindbrain boundary (MHB) and probably derives from this SC population. However, MHB SC and PML progenitors express different markers (glial and neuroepithelial, respectively) (Chapouton et al., 2006) (reviewed by Schmidt et al., 2013).

The zebrafish is a well-established model system for three-dimensional real-time (3D+time) live imaging of morphogenetic events in the eye and nervous system (England et al., 2006; Greiling et al., 2010; Kwan et al., 2012). However, midbrain development remains poorly studied in this organism. The morphogenetic movements that shape the tectum have not been described. Using two-photon laser-scanning microscopy (TPLSM) for imaging neural tissue, and tracking the behaviour of cells in real time, we provide the first comprehensive analysis of the cellular events that shape the OT. We found that the midbrain is formed in a stepwise manner: intense morphogenetic movements shaping the TS (period 1) are followed by continued elongation of the PML and cytological

¹CNRS, UPR3294 Unité Neurobiologie et Développement, F-91198 Gif-sur-Yvette, France. ²MDAM (Multiscale Dynamics in Animal Morphogenesis) group, NED Unit, Institut Fessard, CNRS, F-91198 Gif-sur-Yvette, France. ³INRA, USC1126, F-91198 Gif-sur-Yvette, France. ⁴Institut Pasteur, Macrophages and Development of Immunity, Institut Pasteur, F-75015 Paris, France. ⁵CNRS, URA2578, F-75015 Paris, France. ⁶Université Paris-Sud, F-91400 Orsay, France.

*These authors contributed equally to this work

‡These authors contributed equally to this work

§Authors for correspondence (peyrieras@inaf.cnrs-gif.fr; joly@inaf.cnrs-gif.fr)

Received 14 May 2013; Accepted 25 September 2013

changes without further major morphogenetic movements (period 2). We showed that PML progenitors proliferate slowly by symmetric division. We determined that cells in the PML are slow-amplifying progenitors (SAPs) and turn into fast-amplifying progenitors (FAPs) as they enter into the OT.

Screening expression patterns in the PML allowed us to identify key features of genetic networks that are expressed differentially in progenitors: a network expressed in all proliferating cells (SAP+FAP) and another specific to SAPs. This latter network includes genes involved in ribosome biogenesis and DNA synthesis. We carried out a functional study of the *perplexed* mutant line, which lacks a functional *cad* gene. Our results showed that *cad*, which is strongly expressed only in SAPs, is required more generally for coordinating the cell proliferation and survival of midbrain cells. Therefore, our work leads to the hypothesis that a subset of the ribosome and nucleotide biosynthesis genes, which do not exhibit ubiquitous expression but instead are specific to midbrain SAPs, have a crucial role in proliferating cells during development.

RESULTS

PML morphogenesis occurs in two steps

A histological analysis was carried out on zebrafish embryos from 24 hours post-fertilisation (hpf) to 7 days post-fertilisation (dpf) to study PML morphogenesis. Parasagittal section observations showed that PML can be unambiguously identified in prim-5 stage embryos (24 hpf; end of somitogenesis) (Fig. 1A). At this stage the PML is thick and appears as typical pseudo-stratified neuroepithelium. At 48 hpf (long-pec stage), the PML is a semi-circular layer of cells connecting the OT to more ventral structures originating from the alar neural plate (known as the TS) (Fig. 1C).

There is a similar lateral structure connecting the OT to the TS as seen in transverse sections (not shown). On sagittal sections close to the sagittal plane (Fig. 1D), the medial PML connects the tectum with the medial isthmus proliferation zone, which is itself connected to the cerebellum proliferation zone (CPZ).

The formation of the PML can be divided into two steps: before 48 hpf, the PML undergoes formation as the brain exhibits major morphological changes (period 1); after 48 hpf, the PML structure continues to elongate while the brain grows and the TS and OT become more distant; in addition, PML cells exhibit cytological changes (period 2).

Morphological changes were examined by live imaging of zebrafish embryos expressing nuclear Venus fluorescent protein. Imaging of transverse sections at 26 hpf (during period 1) revealed that, as the tegmentum grows, the TS invaginates and spreads medialwards over the tegmentum from both sides of the embryo (Fig. 1E,F; supplementary material Movie 1). At later stages, proliferation becomes confined to the intermediate zone between the OT and the TS. This lateral proliferation zone becomes marked by slightly more intense staining of the nuclei in the transgenic line. It gradually extends during development and forms the PML between the OT and TS.

We observed no major morphogenetic movements after 48 hpf (period 2); the PML is established and its growth is thereafter coordinated with that of the brain. PML cells undergo prominent cytological changes from a neuroepithelial type (see below) to form a monolayer pavement epithelium. By 7 dpf, these cells are found to be tightly apposed to the posterior side of the OT (Fig. 1A). At this stage, the lateral recesses of the mesencephalic ventricle (located between the tectum and the PML) become invisible (Fig. 1A).

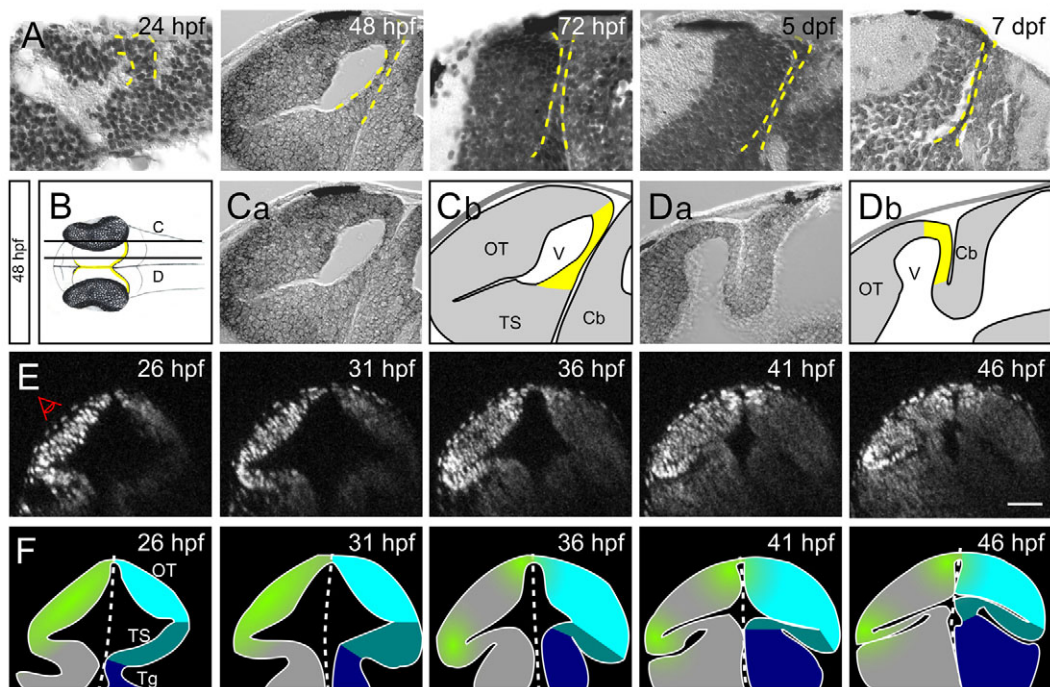


Fig. 1. PML morphogenesis in zebrafish from 1 to 7 dpf. (A) Parasagittal sections of zebrafish from 24 hpf to 7 dpf. As development proceeds, the PML (delineated by a yellow dashed line) becomes thinner and tightly apposed to the OT. (B) Schematic dorsal view of an embryo at 48 hpf. Planes of the sagittal sections in C (more lateral) and D (more medial) are indicated. The PML is found at the margin of the OT (yellow). (C) On lateral sections, the PML connects the OT to the TS. (D) On medial sections, the PML connects the OT to the cerebellum. (E,F) Embryo imaged from its left side (E) and corresponding interpretive schematics (F). Reconstructed midbrain transverse sections were taken at 5-hour intervals. Proliferation (green) becomes restricted to an area between the OT (light blue) and the TS (mid-blue). The tegmentum is in dark blue. Cb, cerebellum; OT, optic tectum; Tg, tegmentum; TS, torus semicircularis; V, ventricle. Scale bar: 50 μ m.

PML cells are large polarised neuroepithelial cells that divide in the planar plane

We examined the localisation of two apical markers in PML cells. At 48 hpf, we found that atypical protein kinase C (aPKC ζ) and Zona occludens protein 1 (ZO-1), which are markers of adherens and tight junctions, respectively, are expressed on the ventricular side (Fig. 2A). We observed that cells of the PML are polarised and have larger nucleoli (Fig. 2B) than those observed in the OT. The chromatin in PML cells appeared decondensed compared with that in OT cells, as shown by electron microscopy (Fig. 2C). Moreover, PML cells exhibited larger and more elongated nuclei, as observed in live imaging (Fig. 2D).

During mitosis, PML cell nuclei transiently swell (Fig. 2E; yellow cells in supplementary material Movie 2) and migrate to the apical side of the layer to divide [interkinetic nuclear migrations (supplementary material Movie 3) (Baye and Link, 2007)]. This is further evidence of the neuroepithelial nature of the PML, as this movement typically occurs during neuroepithelial-like neurogenesis (Götz and Huttner, 2005). We found that most divisions of PML progenitors are within the plane of the neuroepithelium. Most of the observed mitotic events (94.3%) are planar and only a few (5.7%) are apical-basal (Fig. 2F; supplementary material Movie 2, yellow cells divide in a planar fashion). The mitotic plates rotate and then stabilise in orientation shortly before mitosis to achieve planar divisions (supplementary material Fig. S1); this has been described previously in neuroepithelial cells at earlier stages (Herbomel, 1999; Geldmacher-Voss et al., 2003).

PML cells are SAPs and give rise to FAPs of the OT

To directly examine PML and OT cell cycle lengths, we produced TPLSM 3D+time live imaging datasets of nuclear-labelled transgenic zebrafish (supplementary material Fig. S2). Eight PML nuclei were selected at 30 hpf, digitally tagged with Mov-IT software, and individually tracked (Fig. 3A-C; supplementary material Movie 4). After each mitosis, both daughter cells were followed, resulting in a 15-hour lineage analysis with high spatial and temporal accuracy. We measured an average cell cycle length of $5:51 \pm 1:49$ hours ($n=25$) in the PML and a much shorter interval between two mitoses of $1:35 \pm 1:22$ hours ($n=13$) in the OT (Fig. 3G). This shows that, from 30 hpf to 45 hpf, SAPs are located in the PML, whereas FAPs are in the OT. From this lineage analysis we observed that PML cells initially remain in the PML where they divide approximately twice during the whole imaging session (i.e. from 30 hpf to 45 hpf; Fig. 3; an explicit example is given in Fig. 3D-F and in supplementary material Movie 5). Daughter cells are then located around the midbrain ventricle, and at the end of the movie (45 hpf) are seen in the OT (Fig. 3; supplementary material Movies 4, 5). All trajectories are parallel and in the horizontal plane; most of the progeny of any single PML cell remain confined into a small volume in the tectum, such that clonal dispersion is low.

We observed that the progeny of three PML clones contributed to both the OT and the TS [Fig. 3, red (see also supplementary material Movie 6), orange and dark yellow clones].

The PML displays a specific gene expression profile that is shared with the retina CMZ

We looked for potential genetic signatures in PML cells by data mining the ZFIN gene expression database (www.zfin.org/). To distinguish specifically expressed PML genes from those that are more widely expressed in the midbrain (Fig. 4A) we applied several criteria. At the early prim-15 to prim-25 stages (when most tectal cells are still proliferating), expression of a 'thinly' expressed gene

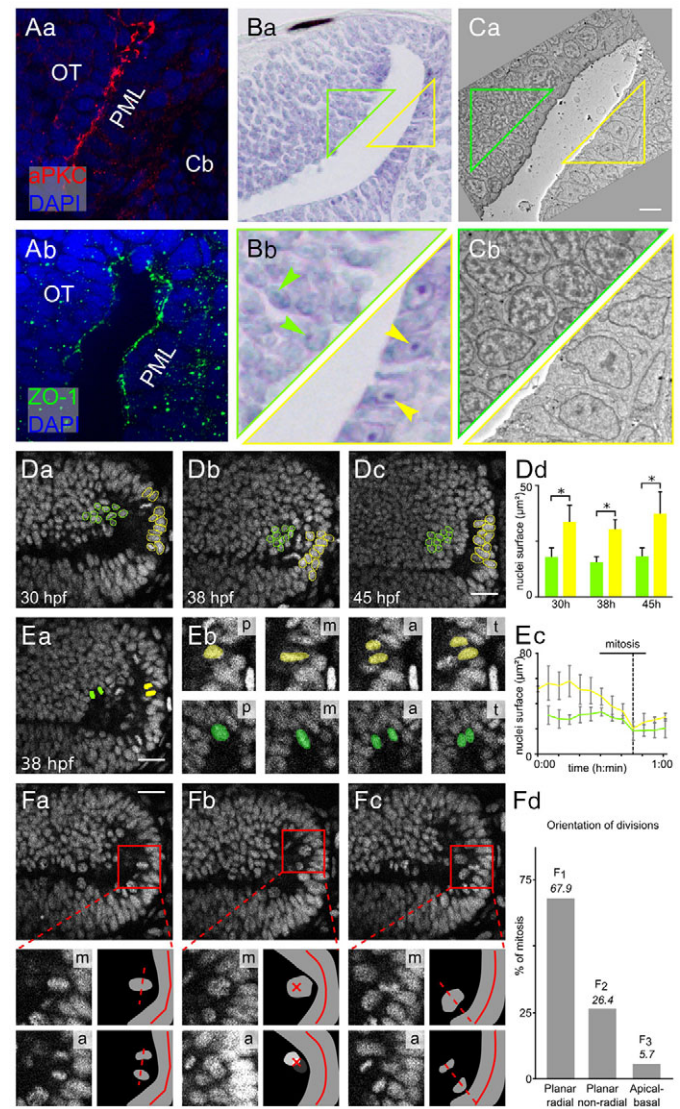


Fig. 2. The PML is a neuroepithelial proliferation zone. (A) Sagittal sections at 48 hpf showing the expression of apical markers in PML cells: aPKC (a) and ZO-1 (b). Nuclei are stained with DAPI. (B) Nissl staining of sagittal sections showing that PML cells (yellow triangle) have larger nuclei with bigger nucleoli than OT cells (green triangle). Arrowheads indicate nucleoli. (C) Electron microscopy image of a sagittal section at 48 hpf showing that PML cells (yellow triangle) have decondensed chromatin, whereas chromatin in OT cells (green triangle) is condensed. (D) Sagittal optical sections of the OT from a *Tg(Xla.Eef1a1:H2B-Venus)* embryo. Interphase nuclei in the PML (yellow) are larger than at the margin of the OT (green). At all stages, the surface areas of the PML and the OT nuclei are significantly different (Mann-Whitney U-test, $*P<0.001$; error bars indicate s.d.). (E) Average PML and OT nucleus size for ten mitoses. (a) Location of tracked nuclei (as detailed in b). p, prophase/prometaphase; m, metaphase; a, anaphase; t, telophase/cytokinesis. (c) M phase is indicated by a dotted line. OT, green; PML, yellow. (F) Mitosis orientations. (a) Planar radial division [30:56 (hours:minutes) hpf]. (b) Planar non-radial division (30:52 hpf). (c) Apicobasal division (31:13 hpf). (Bottom panels) Enlarged metaphase plate (labelled m), subsequent anaphase (labelled a) and corresponding interpretive diagrams. For planar non-radial divisions (b), the two daughter cells are not in the same plane. The anaphase image is the sum of the images centred on the two daughter cells. The red cross indicates the axes of the planar non-radial mitoses. Of 53 mitoses, 36 are planar radial, 14 are planar non-radial and 3 are apicobasal. (d) Non-random predominantly planar radial mitoses according to χ^2 test ($P<0.001$). Cb, cerebellum; OT, optic tectum; PML, peripheral midbrain layer. Scale bars: 20 μ m.

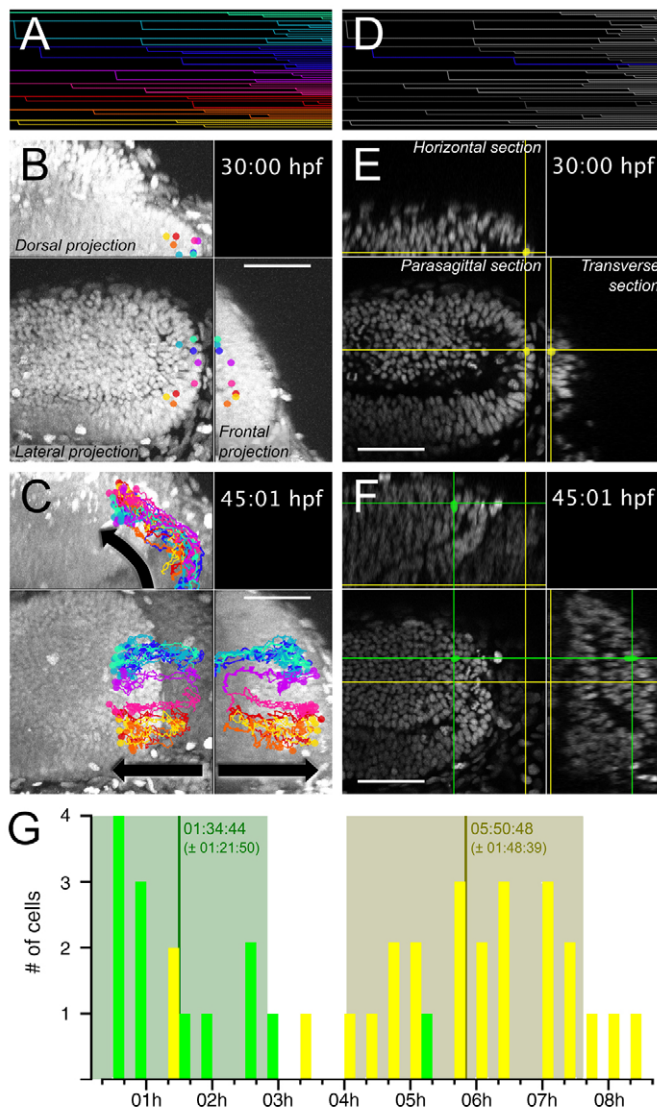


Fig. 3. Slow-amplifying PML cells give rise to tectal FAPs. PML cells were tracked from 30:00 hpf to 45:01 hpf. The complete lineage tree is shown in A. Cells originating from the PML at 30 hpf are found in the external part of the OT 15 hours later (B,C). In B and C, eight clonal cell trajectories, as indicated with different colours, have been overlaid on a volume projection of the left midbrain. The dots indicate the position of the cells at 30 hpf (B) and 45:01 hpf (C) and the lines trace the past trajectory of each clone. For the full movie, see supplementary material Movie 4. (D-F) A clone (represented by the intersection of the cross at the corresponding sagittal, horizontal and transverse planes) is followed from the PML, where it achieved two mitoses (E), to the OT, where two further mitoses occurred (F). For the full movie, see supplementary material Movie 5. (G) Cell cycle durations are separated into two clusters: OT (green) FAP cycles, $1:35 \pm 1:22$ hours ($n=13$); PML (yellow) SAP cycles, $5:51 \pm 1:49$ hours ($n=25$). Scale bars: 50 μ m.

had to be restricted to the peripheral part of the midbrain and not be ubiquitously expressed throughout the whole proliferating midbrain (in the way that proliferation-associated markers are at that stage). At later stages (high-pec to long-pec) the midbrain expression domain had to be thin and restricted to the PML in Nomarski images. Since a striking synexpression in tectum and retina was observed (see below), we also used another criterion: the identification of a ring of retina cells tightly surrounding the lens. More widely expressed genes, associated with all progenitors, are expressed in a wider ring corresponding to proliferative cells of the

CMZ (supplementary material Fig. S3). We found 117 genes associated with proliferation (supplementary material Fig. S3, Table S1). Of these, 68 genes are expressed in a relatively large region of the peripheral OT and of the CMZ, whereas 49 display a very thin expression pattern located at the most peripheral part of the OT and in the most central part of the CMZ (supplementary material Fig. S3). We also added a further two genes to this second category: *ect2* and *nop56* (*nol5a*) (supplementary material Table S1). These were identified from a previous *in situ* hybridisation screening performed on medaka (data not shown) and their specific expression was also confirmed in zebrafish (Fig. 4Ae,f,Cb,c). ZFIN data mining results are presented in supplementary material Fig. S3.

We carried out whole-mount *in situ* hybridisation (WMISH) and histological analysis on a subset of proliferation-associated genes to confirm the data mining results. We identified a group of genes, which included *pcna*, with expression that encompasses both FAPs and SAPs (Fig. 4Aa-c). Other genes, such as *nop56*, display a tight expression pattern that is restricted to PML SAPs (Fig. 4Ad-f). We carefully checked that these PML-associated patterns correlate with expression in SAPs. We found that transcripts of the *pescadillo* (*pes*) gene specifically localise in neuroepithelial cells with large oval nuclei – cells that we called SAPs (Fig. 4B). We also performed WMISH for four genes (*cad*, *ect2*, *nop56* and *pes*; see Fig. 4C) with a very long incubation time (several days) in the staining solution to demonstrate that PML gene expression patterns are really restricted to SAPs.

Two main gene categories are overrepresented in the PML-specific dataset

To define groups of genes with similar functions, we performed several *in silico* analyses. Gene Ontology (GO) term analyses show that, in both of our lists, genes regulating specific cellular functions are overrepresented (Fig. 5; supplementary material Fig. S4). Most genes associated with the proliferation zones of the OT and the PML encode components of the nucleus linked to the global proliferation machinery, more specifically to the machinery regulating cell cycle phases or DNA replication (supplementary material Fig. S4). By contrast, the PML dataset contains mainly genes encoding either nuclear proteins that are active in nucleotide synthesis or nucleolar proteins (Fig. 5A,B). An interaction network analysis using Ingenuity software identified several clusters of PML-specific genes (Fig. 5C), one of which corresponds to a subset of genes encoding proteins involved in rRNA processing (such as *nop56*, *nop58*, *fibrillarin*, *pes*, *wdr12* and *nle1*) (Fig. 5C; supplementary material Table S1).

Interestingly, gene networks already identified by a functional RNAi screen as crucial for *Drosophila* neuroblasts are very similar to the PML progenitor-specific networks (supplementary material Fig. S4) (Neumüller et al., 2011). To test the relevance of our dataset with other SC sets, we compared the identified genes with previously assembled mammalian datasets by searching the Molecular Signature Database MSigDB (v3.0) (Subramanian et al., 2005). Our set of PML-specific genes is enriched for genes that are represented in different cancer-associated gene sets (supplementary material Table S2) and, more importantly, in the PluriNet network (Müller et al., 2008) related to human pluripotent stem cells. This study (Müller et al., 2008) indicates that pluripotent cells exhibit a small number of generic molecular signatures, the functions of which are often linked to the maintenance of pluripotency.

The proliferation and survival of tectal progenitors are affected in the perplexed mutant

Many genes considered as housekeeping genes exhibit preferential expression in the PML. To test whether these genes play specific

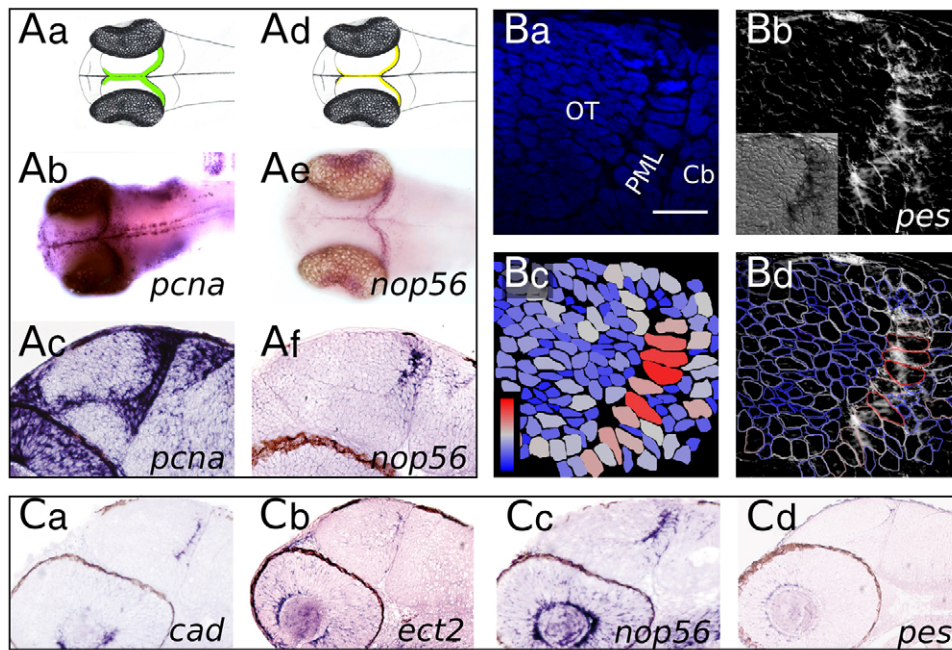


Fig. 4. Transcript distribution in the midbrain: 'large' and 'thin' domains. (A) Whole-mount embryos (b,e) and parasagittal sections (c,f) following *in situ* hybridisation (ISH) with *pcna* (b,c) and *nop56* (e,f) probes. *pcna* is expressed in a 'large' domain containing all proliferating cells. The *nop56* expression domain is 'thin' and restricted to PML SAPs. (B) The *pes* ISH signal colocalises with PML cells (the largest midbrain cells). (a) Nuclear DAPI staining. (b) Inverted colour brightfield image of the same field showing the *pes* ISH signal. Inset shows the real colour brightfield image. (c) Colour-coded nuclei surface. On the blue-red scale, red corresponds to 22 μm^2 and dark blue to 0 μm^2 . (d) Overlay of the inverted brightfield image with the nuclei border colour-coded drawing. Red nuclei exhibit a strong *pes* ISH signal. (C) Sagittal sections of embryos at 2 dpf. ISH long staining time emphasizes PML-specific gene expression. Scale bar: 10 μm .

roles in PML progenitors, we performed an analysis of the *perplexed* mutant, which lacks a functional *cad* (*carbamoyl-phosphate synthetase 2, aspartate transcarbamylase, and dihydroorotase*) gene, which encodes three enzymes involved in *de novo* pyrimidine biosynthesis (Willer et al., 2005). At 48 hpf, we observed that the PML and OT remain recognisable in *perplexed* mutants but their morphologies are strongly affected. The PML appears thicker than in wild-type embryos (Fig. 6A,B). Throughout the midbrain region, the density of cells is low and there are numerous acellular holes. We imaged midbrains of *perplexed* mutants by TPLSM, but apoptosis rates were so high that we were not able to track cells for an entire cell cycle (data not shown). Massive cell death was detected in mutant OT after TUNEL staining (Fig. 6C,D). We monitored proliferation levels by phospho-histone H3 (pH3) immunostaining at 48 hpf. M-phase cells are present in the proliferative areas (FAP areas) of the tectum and of the TS in *perplexed* mutants (Fig. 6E,F). However, more M-phase cells are visible in the central part of the OT in mutants than in wild types. This was confirmed by Pcn immunostaining at later stages (72 and 96 hpf), when proliferation zones become narrower. In wild type, Pcn expression is restricted to the margin of the OT (FAPs) and PML (SAPs), whereas in *perplexed* mutants Pcn-positive cells are found throughout the whole OT and cerebellum (Fig. 6G-J).

DISCUSSION

The PML is formed of neuroepithelial SAPs that give rise to both OT and TS

We have shown in this study that PML cells exhibit the prototypical features of neuroepithelial progenitors. Located in the largest structure of the fish brain (the OT), PML cells are particularly suitable for studies of the functional and structural characteristics of NPs. We provide an extended description of PML progenitors and highlight how the teleost PML can be used as a model for the characterisation of molecular pathways acting in neuroepithelial SAPs.

The large majority of cell divisions occurring in the PML are planar divisions, although we observed a few apicobasal divisions. In the zebrafish telencephalon, radial glial cells predominantly undergo

symmetric gliogenic divisions, which amplify the NSC pool (Rothenaigner et al., 2011). The reason why fish seem to preferentially use this growth mode remains unknown, but it has been shown that a planar orientation of mitoses in neuroepithelia is required for the maintenance of layered structures (Peyre et al., 2011).

We demonstrated that the cell cycle takes about four times longer in the PML than in the OT. To understand the biology of these SAPs, it will be important to identify the factors that induce this relative quiescence in PML cells (see below).

Cells exhibit a major cytological transition when they enter the tectum: from a neuroepithelial phenotype, establishing contacts with the ventricle (apically) and with the pial/basal membrane, to small round cells that sometimes lack contacts with either the pial/basal membrane or the ventricle (data not shown). This transition is apparently correlated with a substantial shift in proliferation rates. It will be interesting to study the factors, positions or cell contacts that trigger this major phenotypic transition. Several well-known signalling molecules are known to induce a fast proliferation mode. For example, sonic hedgehog (Shh) may have a prominent role in the acceleration of cell divisions, as it does in the retina (Locker et al., 2006). The control of progenitor proliferation in the tectum has been shown to be substantially affected in several mutants of the hedgehog pathway (Koudijs et al., 2005).

Our results confirm on live specimens that the OT is a typical cellular conveyor belt (Devès and Bourrat, 2012); it has zones of unmixed FAPs and SAPs at its periphery, a zone of cells exiting the cycle and a central zone of differentiating cells (Cerveny et al., 2012) (Fig. 7). Our data show centripetal movements of the progenitors when they enter the tectum. However, we believe that these movements are not due to active migration but rather to passive displacements resulting from intensive cell division. It would be interesting to analyse more globally the major directions of cell displacements that shape the OT, PML and TS (using automated cell tracking and visualisation of kinematic descriptor maps).

None of the tracked cells remains in the PML to replenish the SAPs. One hypothesis is that the bona fide SCs of the PML are localised more medially in the isthmus proliferation zone and

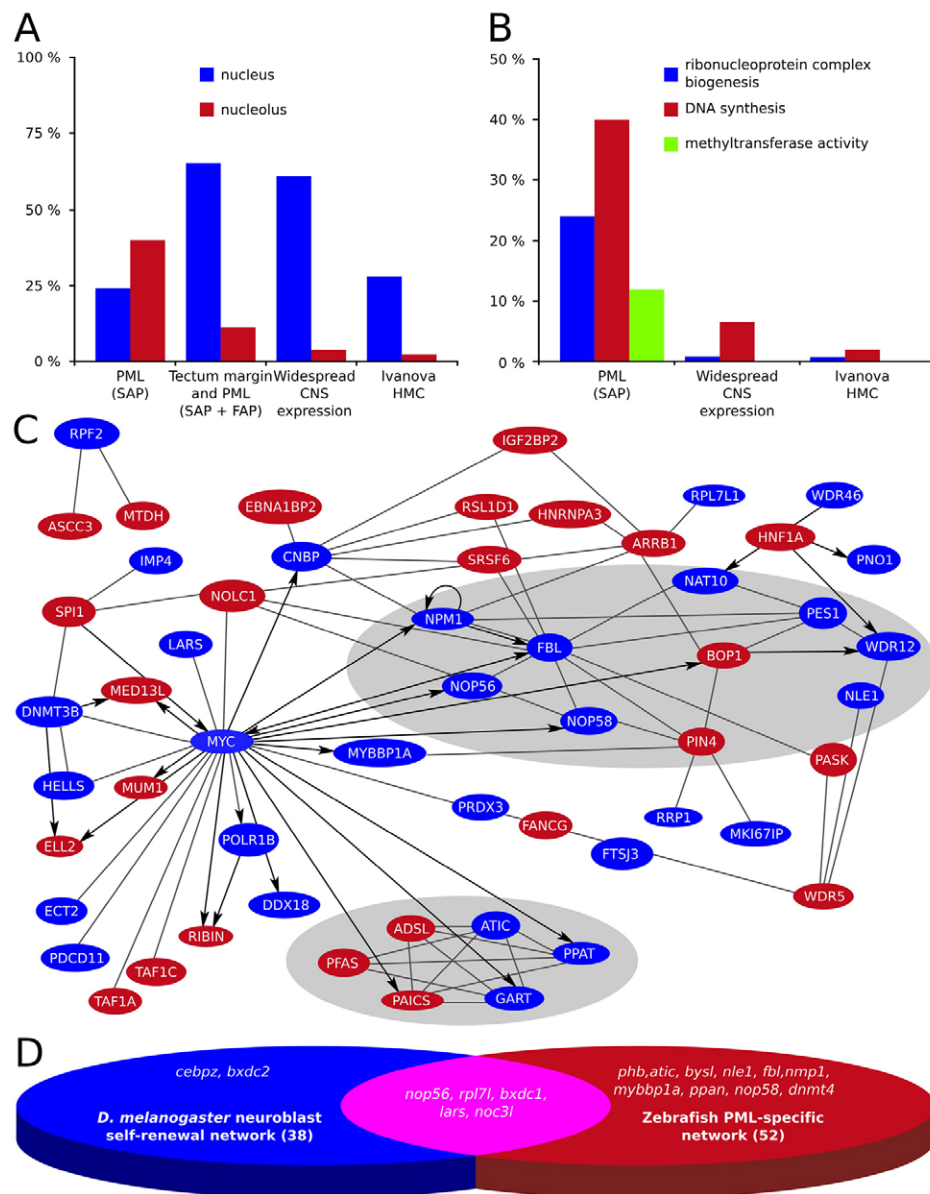


Fig. 5. The PML gene network contains genes encoding nucleotide biosynthesis enzymes, nucleolar components and ribosomal proteins. (A,B) Gene ontology (GO) enrichment analysis of the PML-specific gene list, using the CNS and Ivanova hematopoiesis mature cells (HMC) gene lists as backgrounds. (A) Cellular localisation: genes encoding nucleolar proteins are overrepresented in the PML dataset. (B) Cellular function: in the PML dataset, genes involved in ribosome biogenesis and nucleotide synthesis are overrepresented. (C) Ingenuity pathway analysis of the main gene network for the PML dataset. Two distinct molecular clusters are outlined (grey): nuclear proteins mainly involve purine biosynthesis, and nucleolar proteins involve rRNA and ribosomal processing. PML genes are in blue and genes not included in our study are in red. Arrows starting from *myc* indicate direct Myc target genes or partners. (D) Overlap between fish and *Drosophila* NSC lists.

correspond to the *her5*-positive population described by Chapouton et al. (Chapouton et al., 2006).

We found that the PML contains a subset of progenitors that gives rise to both the OT and TS. It is striking that a single progenitor is able to generate cells belonging to two distinct brain structures. This unusual and unexpected dual contribution seems to be dependent on the location of the tracked progenitor in the PML with respect to the dorsoventral axis. This feature was already proposed by Grandel et al. (Grandel et al., 2006), who noted that the TS has no specific zone of progenitors. However, their study was performed on adults and did not provide any evidence for the location of early TS progenitors. In the mouse embryo, some progenitors have the capacity to populate more than one neural structure; for example, the diencephalon and telencephalon (Mathis and Nicolas, 2006).

PML cells express genes active in stem cells and tumour cells

Pluripotent embryonic SCs have the widest possible capability for gene transcription. As they become more specialised, they refine their transcriptional repertoire (Efroni et al., 2008). In our model of

pluripotent neural cells (the SAP/PML cells), we identified different groups of genes as described below according to the function they fulfil.

One PML cell-specific group contains genes known to play major functions in SCs and tumour cells, where they either contribute to the regulation of DNA methylation (*dnmt4* and *hells*) (Law and Jacobsen, 2010) or inhibit cell apoptosis (*ppan*) (Bugner et al., 2011).

PML cells also express *bystin* transcripts that have been reported to be expressed in type B SCs and in lesioned rat cerebral cortex (Sheng et al., 2004).

Prohibitin (Phb), which is often associated with cancer, is an inhibitor of cell proliferation (Mishra et al., 2006) that could potentially trigger the slowing of progenitor cell divisions. Indeed, genes known to promote definitive cell cycle exit in the differentiating cells of the OT [such as cyclin-dependant kinase inhibitors, *gadd45* or *insm1* (Candal et al., 2004; Candal et al., 2007)] were found not to be expressed in PML progenitors (data not shown). This suggests that the mechanisms inducing quiescence in SCs are distinct from those promoting cell cycle exit during terminal differentiation.

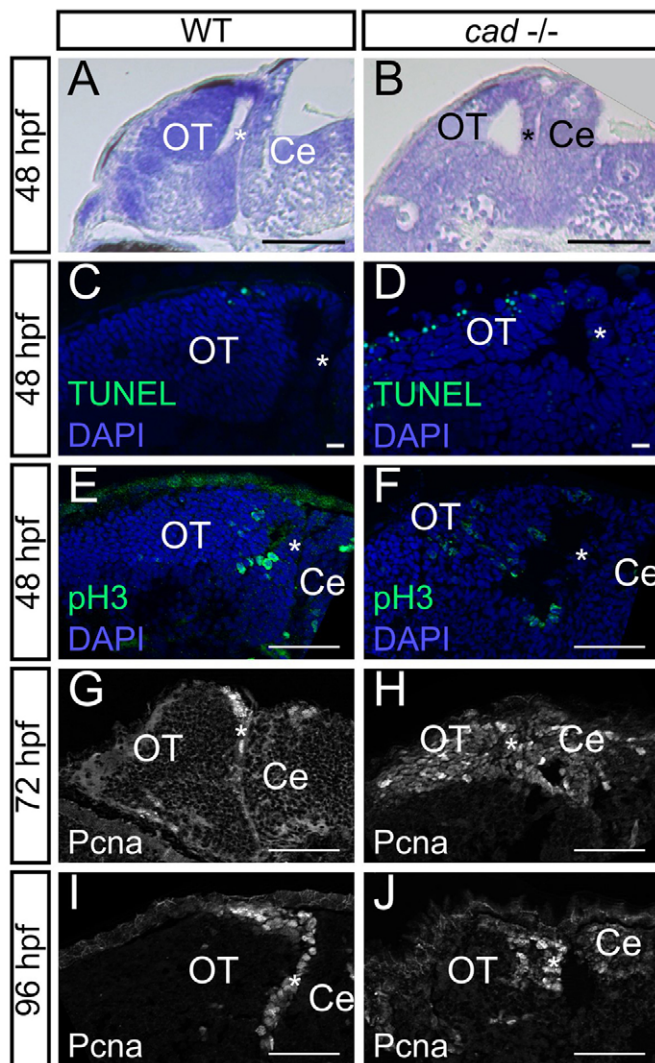


Fig. 6. Absence of *cad* function in homozygous mutant embryos leads to proliferation defects and massive cell death in the midbrain.

(A,B) Sagittal sections of wild-type (A) and *perplexed* (B) embryos with Nissl staining at 48 hpf. *perplexed* mutant displays atrophy of the tectum and PML thickening. (C,D) Sagittal sections following TUNEL staining at 48 hpf. More apoptotic cells are observed in *cad*^{-/-} (D) than in wild-type (C) embryos. (E,F) Phospho-histone H3 labelling at 48 hpf showing the presence of proliferative cells not only in the periphery of the tectum but also in the central part in *perplexed* mutants. (G-J) PcnA immunostaining at 72 and 96 hpf showing persistence of wide proliferation zones in the OT of *perplexed* mutants at late larva stages. Anterior is at the left and dorsal at the top of each image. OT, optic tectum; Ce, cerebellum. The asterisk indicates the PML. Scale bars: 100 μ m in A,B; 10 μ m in C,D; 20 μ m in G; 50 μ m in E,F,H-J.

Among the PML cell-specific gene network we identified *c-myc* (*myca* in zebrafish), which is known to be a master regulator of normal cell growth and proliferation (Liu et al., 2008) (Fig. 5D; supplementary material Fig. S3Y2,4) and could play a specific role in SAPs. In *Xenopus*, *c-myc*^{+/+}/*n-myc*^{-/-} cells were shown to be candidates for a restricted population of retinal SCs found in a subdomain at the tip of the CMZ (Xue and Harris, 2011). Transcripts of several Myc targets are also restricted to the PML (see below; Fig. 5). The gene *mybbp1a* is located at a key node of the established PML network. This gene has been shown to activate *p53* when ribosome biogenesis is suppressed (Tsuchiya et al., 2011) and *Mybbp1a* might be part of a nucleolar pool of proteins involved in mitotic progression (Perrera et

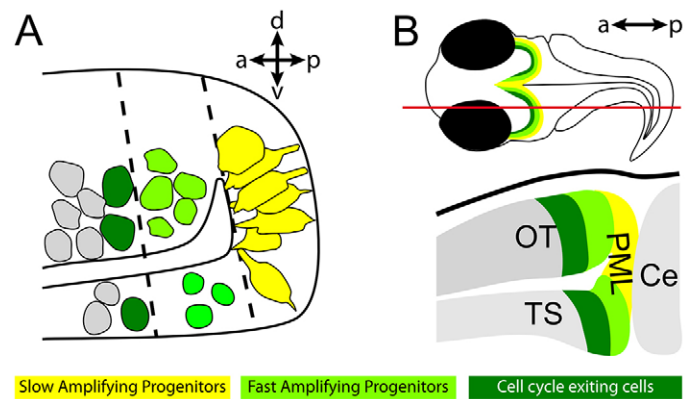


Fig. 7. The PML contributes to the formation of the OT and of the TS.

(A) At the periphery of the OT, there are two types of neural progenitors. PML cells (yellow) are SAPs and have big nuclei and contact both apical and basal with membrane extensions. They turn into SAPs (light green) with smaller nuclei when they enter the OT or the TS, then they exit the cell cycle (dark green) and differentiate. (B) Top panel: the previously described differentiation gradient forms a concentric gradation when viewed in horizontal section and correlates with observed gene expression patterns. Red line indicates the parasagittal section shown in the bottom panel. OT, optic tectum; TS, torus semicircularis; Ce, cerebellum; PML, peripheral midbrain layer.

al., 2010). Further studies are needed to clarify the role of *Mybbp1a* in NSCs and SAPs by focusing on the interplay between its nucleolar and cell cycle-associated functions.

Other genes found to be specifically expressed in the PML encode nucleotide biosynthesis enzymes, nucleolar components and ribosomal proteins.

A large PML-specific gene network encodes nucleolar proteins

Genes encoding nucleolar proteins are present in the PML network. Cancer studies have proposed putative instructive roles for nucleolar proteins in tumorigenesis, highlighting their potential role in the control of cell proliferation (reviewed by Ruggero and Pandolfi, 2003). PML nucleolar genes encode proteins belonging to two main complexes. Nop56, Nop58 and Fibrillarin are small nucleolar ribonucleoproteins (SnoRNPs) that are associated in a complex involved in the processing and modification of rRNA. Transcripts encoding Nop56/58 are signatures of fish PML progenitors (this study), but also of the fish (Fig. 5) and *Xenopus* (Parain et al., 2011) retina. The Wdr12, Pes and Bop1 proteins are associated with PeBoW, a complex crucial for the maturation of the large ribosomal subunits in mammalian cells (Hölzel et al., 2005). *pes* was first identified in zebrafish for promoting proliferation in the CNS (Allende et al., 1996). *nle1* and *wdr12* are involved in the biogenesis of ribosomal pre-60S particles. Interestingly, *nle1* is also required for the maintenance of adult hematopoietic stem cells (HSCs) in mice, as shown by conditional knockouts (Le Boutellier et al., 2013).

The expression of genes coding for ribosomal protein is crucial in SCs and SAPs

Ribosomal genes are thought to be ubiquitously expressed and to have strong and early deleterious effects. It is therefore surprising to observe that PML genes encoding ribosomal proteins have restricted transcription patterns and that some have a mild mutant phenotype. For example, zebrafish *rpl71l* is specifically expressed in PML and CMZ progenitors (supplementary material Fig. S4) and the *rpl71l* mutant apparently has a mild phenotype (source: ZIRC). By contrast,

its paralogue *rpl7* has been demonstrated to be strongly and ubiquitously expressed (Bradford et al., 2011). A similar situation might occur in *Drosophila*, where *RpL7* has been shown to be specifically required in neuroblasts to maintain their proliferation (Neumüller et al., 2011), whereas its counterpart (*RpL7-like*) displays ubiquitous expression. Another zebrafish study shows that *rpl22l1* and *rpl22* play essential, distinct and antagonistic roles in HSCs (Zhang et al., 2013). Since protein synthesis does not seem to be affected in mutants, these two genes might have some extra-ribosomal functions in the regulation of HSCs. Proteins regulating ribosome synthesis seem to be essential for germline stem cell (GSC) maintenance and function in the gonads of *Drosophila* (Fichelson et al., 2009). The accumulation of specific ribosomal proteins in PML cells creates a signature that distinguishes SAPs from FAPs and other cells of the OT. Recent discoveries of ribosome codes in yeast (Komili et al., 2007) and vertebrates (Kondrashov et al., 2011) highlight the importance of such gene expression signatures.

A PML gene network encodes nucleotide biosynthesis enzymes

One PML cluster contains genes involved in pathways of purine synthesis (such as *gart*, *ppat*, *atic*), pyrimidine biosynthesis [such as *cad* (see also below) and *ctps1a*] and nucleotide metabolism (such as *shmt2*, which has been shown to be regulated by *myc*) (Fig. 5; supplementary material Table S1). It is surprising that transcripts encoding nucleotide biosynthesis proteins accumulate only in SAPs and not in all proliferating cells. In cell culture, *cad* activity is strongly upregulated when cells enter the proliferative phase, and then dramatically downregulated as the culture becomes confluent (Sigoillot et al., 2002).

Are PML cells storage chambers?

We chose to analyse the *perplexed* mutant, which lacks a functional *cad* gene, because a previous study carried out in the retina had already highlighted the importance of this gene for NP proliferation and differentiation (Willer et al., 2005). *perplexed* mutants exhibit no lamination of the retina (Link et al., 2001; Willer et al., 2005). Similarly, we observed that they lack a laminated tectum. The presence of a large number of PcnA-positive cells all over the OT indicates that the cell cycle is dysregulated in midbrain progenitors. In time-lapse analysis, cell cycle intervals could not be precisely measured owing to massive apoptosis in mutant OT. Hence, our hypothesis is that, in *perplexed* mutants, because of the absence of *de novo* nucleoside synthesis, tectal cells, as with retinal cells (Willer et al., 2005), do not undergo proper mitoses and remain blocked in M phase and eventually undergo apoptosis. Indeed, in the eye it has been shown that retinoblasts with the *perplexed* mutation require twice as long to complete one cell cycle (Willer et al., 2005). It is known that the *de novo* pathway of pyrimidine synthesis is most active during growth and development, after which the salvage pathway predominates (Anderson and Parkinson, 1997). Since metabolic intermediates along this pathway do not accumulate, the level of uridine monophosphate (UMP) production relies on *Cad* activity. Thus, we propose that neuroepithelial cells accumulate high levels of *Cad* enzymes so that OT FAPs can subsequently perform their rapid divisions without *de novo* synthesis of nucleotides. More generally, the accumulation of machineries composed of many different nucleolar/ribosomal proteins or nuclear proteins might point to key roles for these proteins in the biology of these slowly dividing cells, which have high transcriptional and translational activity (Efroni et al., 2008). We speculate that PML cells, which are poised for subsequent rapid divisions, serve as ‘storage chambers’

and thus allow the FAPs to bypass *de novo* synthesis during their intense proliferative activity. This would be similar to the early development strategy whereby maternal components are stored in the huge pluripotent egg cell in readiness for subsequent rapid divisions of the blastomeres.

PML genes are also expressed in the CMZ: evidence of deep homology?

Other PML genes could also have a prominent function in the fish midbrain and eye. Cytological and molecular signatures may help to define cell type homologies from an ‘evo-devo’ perspective (Arendt, 2005). Synexpression of genes in retinal CMZ cells and midbrain progenitors has been noted (Cervený et al., 2012; Ramialison et al., 2012) and the phenotypes of mutants for at least 18 PML-specific genes are illustrated on the ZIRC website (supplementary material Table S3). These mutants share strikingly similar neuroectodermal and ocular defects. Heads and eyes appear smaller and necrosis is often reported in the CNS. Further analyses of these mutants are needed to confirm whether these PML genes affect the midbrain neuroepithelial progenitors, in the way that *cad* does.

At early stages of development, more than one-third of the PML-specific genes (according to the ZFIN database) are expressed in the anterior brain region located between the zona limitans intrathalamica and the MHB. This area is proposed to have derived from that of an ancient bilaterian ancestor (Steinmetz et al., 2011). From an initial situation in urbilateria in which rows of lateral (so-called intermediate) progenitors would have participated in both alar forebrain and midbrain morphogenesis, extant vertebrates now evaginate optic cups and their progenitor zone, called the CMZ, whereas the midbrain progenitors in the PML invaginate as revealed in this study. We therefore suggest that retina and midbrain progenitors might be ‘sister’ cell types with a common evolutionary origin.

Conclusions

We have characterised a population of neuroepithelial midbrain progenitors in zebrafish embryos. Their specific features (long cell cycles, distinctive genetic signatures) emphasize the diversity of NPs in vertebrates. Our work highlights that the PML provides a very useful model with which to study NPs and NSCs. Indeed, we propose that these progenitors have specific metabolic activities and use specific ribosome biogenesis pathways. Future studies should also reinforce interest in this cell type by stressing its role in regenerative processes or in modified nutritional contexts.

MATERIALS AND METHODS

Fish

Zebrafish (*Danio rerio*) wild-type strains (AB and TU) and *perplexed* mutants (*cad^{u52}*) (ZIRC, Eugene, OR, USA) were reared and staged as previously described (Kimmel et al., 1995). For wild-type live imaging, we used a transgenic fish line *Tg(Xla.Eef1a1:H2B-Venus)* to track nuclei. Additionally, we used a double-transgenic fish line resulting from a cross between *Tg(Xla.Eef1a1:H2B-mCherry)* (gift from Georges Lutfalla, Université Montpellier 2, Montpellier, France) and *Tg(Xla.Eef1a1:EGFP-Hsa.HRAS)*.

Two-photon live imaging

To avoid pigmentation zebrafish embryos were treated with 1-phenyl 2-thiourea (0.003%; Sigma), anaesthetised with tricaine (170 µg/ml; Sigma), dechorionated, mounted in 1% standard agarose moulds and covered with 0.5% low melting point agarose. Embryos were imaged laterally and imaging field was focused on the left midbrain. Non-invasiveness was assessed by comparing mitosis between TPLSM and Nomarski imaging (supplementary material Fig. S1). Live imaging was performed using

custom-made two-photon microscopes (BioEmergences). The set-ups are based on a DM6000 and a DM5000 upright microscope (Leica) with 980 nm (Mai Tai, Spectra-Physics/Newport Corporation) and 1030 nm (t-Pulse, Amplitude Systems) excitation wavelengths. Other settings/parameters: objectives, Leica 1.0 NA 20× W (HCX APO) or Olympus 0.95 NA 20× W (XLUMPlanFluo); filters, 525/50 nm (Venus and EGFP), 610/75 nm or 595/45 nm (mCherry); scan speed, 700 Hz; frame average, 3; 512×512 pixels at 0.3 or 0.4 µm wide; a full z-stack was compiled in ~5 minutes. To check that imaging was not deleterious, larvae were allowed to recover in tricaine-free embryo medium until able to feed.

3D+time image analysis

After acquisition, raw images were converted into VTK format and processed with Fiji for rendering and other analysis. We also used the Mov-IT software developed by BioEmergences (Olivier et al., 2010), which enables smooth navigation in orthoslices or in volume rendering acquired at different times, fate map visualisation, and the export of lineage trees with all quantitative information related to cellular dynamics.

Electron microscopy

Zebrafish embryos were anaesthetised at 48 hpf in tricaine (170 µg/ml; Sigma) and rapidly prefixed in fixative A (2.5% paraformaldehyde and 2.5% glutaraldehyde in 0.1 M sodium cacodylate buffer pH 7.2). Embryo heads were dissected and prefixed in fixative A for 12–18 hours at 4°C and then embedded in 1% low melting point agarose and oriented in agarose cubes (<1 mm³). Heads were kept at 4°C and prefixed for a further 12–18 hours. After infiltration in Epon 812 (Electron Microscopy Sciences), blocks were oriented in moulds and left to polymerise for 48 hours at 60°C. Sections (50–60 nm) were cut using a Leica EM UC6 ultramicrotome and a Diatome Histo-Jumbo diamond knife. After intensification in uranyl acetate and lead citrate, the sections were observed using a JEOL 1400 electron microscope (120 kV) and pictures were taken using a SC1000 Orius GATAN camera.

Histology

Whole-mount *in situ* hybridisation (WMISH) was performed as previously described (Xu et al., 1994). Antisense riboprobes and paraffin sections were prepared as previously described (Brombin et al., 2011). Sequences of the DIG riboprobes used for *in situ* hybridisation are given in supplementary material Table S4. Brightfield imaging was performed with a Leica DMRD microscope (Nikon Eclipse E800 camera) or a Nikon AZ100 microscope (Nikon Digital Sight DSRi1). For cryosections, embryos were first protected by incubation in 30% sucrose in phosphate-buffered saline (PBS) for 12–16 hours at 4°C, then embedded in OCT Compound (Sakura), stored at –80°C, and sectioned at 14 µm using a Leica cryostat. Antisera were rabbit anti-phospho-H3 (1:1000; CR10, Millipore), rabbit anti-aPKCζ (1:200; C-20, sc-216, Santa Cruz Biotechnology), mouse anti-ZO-1 (1:100; 1A12, Molecular Probes, Life Technologies) and mouse anti-Pcna (1:200; PC10, DAKO); secondary antibodies were AlexaFluor 488 or AlexaFluor 568 goat anti-mouse or goat anti-rabbit conjugates (1:200; Molecular Probes). Sections were mounted in Prolong Gold Antifade Reagent including DAPI (Invitrogen) and imaged with a Zeiss AxioImager M2 microscope equipped with ApoTome.

TUNEL labelling was performed using the Deadend Fluorometric TUNEL system (Promega) according to manufacturer's instructions. Sections were washed in PBS, counterstained with DAPI (Sigma) and mounted with Vectashield hard-set mounting medium (Vector Laboratories).

Bioinformatic analyses

All homology searches and gene annotations were carried out using the Blast2GO functional analysis suite (<http://www.blast2go.com/b2ghome>; B2G) (Conesa et al., 2005). An InterPro scan was performed to find functional motifs and related GO terms using the specific tool implemented in the Blast2GO software (with the default parameters). We used Fisher's exact test for the statistical analysis of GO term frequency differences between two sets of sequences identified with Enrichment Analysis tools. We used a gene list expressed in whole zebrafish CNS (data mined in ZFIN by Yan Jaszczyszyn, personal communication), together with the Ivanova hematopoiesis mature cells list of genes upregulated in mature blood

cells from adult bone marrow and fetal liver, as backgrounds for enrichment analysis. These lists are available in MSigDB v3.0 (<http://www.broadinstitute.org/gsea/msigdb/index.jsp>).

Ingenuity pathway analysis software (Ingenuity Systems) was used to generate networks based on their connectivity in the bibliography and in microarray experiments.

Acknowledgements

We thank Audrey Colin, Laurent Legendre and Matthieu Simion for excellent fish care; Jean-Yves Tiercelin and Patrick Para for expert technical assistance; Ingrid Colin, Vasily Gurchenkov and Ludovic Leconte for help in molecular biology or microscopy; Maximilian Haeussler and Olivier Mirabeau for help with the *in silico* analysis; Yan Jaszczyszyn for providing a CNS gene list; and Pierre Boudinot for help with the Ingenuity pathway analysis. Bernard and Christine Thisse and the ZFIN members are acknowledged for their excellent *in situ* hybridisation database and for allowing us to publish pictures extracted from ZFIN. The AMAGEN, BioEmergences-IBISA-FBI and IMAGIF platforms are thanked for their excellent services in transgenesis and imaging. We have learned a great deal from all our colleagues and gratefully acknowledge our debt to them, in particular: Guillaume Carita, Karine Badonnel, Sylvia Bruneau, Alberta Palazzo, Frédéric Sohm and Michel Cohen-Tannoudji. We thank Alessandro Lunni, Jakob von Trotha, Georges Lutfalla and Michel Vervoort for reviewing the earlier version of the manuscript.

Competing interests

The authors declare no competing financial interests.

Author contributions

G.R. carried out live imaging and image analysis with the help of N.P. and T.S. who conceived Mov-IT software, and assembled the figures. J.J., A.B., A.H., E.M., F.B. and F.J. performed molecular biology and histology experiments. J.-M.H. performed electron microscopy experiments. S.D. generated the zebrafish fluorescent transgenic lines. P.H. performed the Nomarski movie. J.J. and J.-S.J. performed the datamining and gene network analysis. G.R., J.J., A.B., A.H., E.M., F.J. and J.-S.J. analysed the data and assembled the manuscript. F.J., J.-S.J. and N.P. conceived the study. G.R., F.J. and J.-S.J. wrote the manuscript with contributions from J.J., A.B., A.H., E.M., J.-M.H., F.B. and N.P.

Funding

We acknowledge support from Centre national de la recherche scientifique (CNRS), Institut national de la recherche agronomique (INRA), Institut national de la santé et de la recherche médicale (INSERM), Université Paris Sud, Agence Nationale de la Recherche and the European Commission [STREP Plurigenes, CISSTEM, FP6 NEST program (Embryomics and BioEmergences EC projects) and FP7 Health program (zf-Health project) to N.P.].

Supplementary material

Supplementary material available online at <http://dev.biologists.org/lookup/suppl/doi:10.1242/dev.099010/-/DC1>

References

- Allende, M. L., Amsterdam, A., Becker, T., Kawakami, K., Gaiano, N. and Hopkins, N. (1996). Insertional mutagenesis in zebrafish identifies two novel genes, *pescadillo* and *dead eye*, essential for embryonic development. *Genes Dev.* **10**, 3141–3155.
- Alunni, A., Hermel, J. M., Heuzé, A., Bourrat, F., Jamen, F. and Joly, J. S. (2010). Evidence for neural stem cells in the medaka optic tectum proliferation zones. *Dev. Neurobiol.* **70**, 693–713.
- Amsterdam, A., Burgess, S., Golling, G., Chen, W., Sun, Z., Townsend, K., Farrington, S., Haldi, M. and Hopkins, N. (1999). A large-scale insertional mutagenesis screen in zebrafish. *Genes Dev.* **13**, 2713–2724.
- Anderson, C. M. and Parkinson, F. E. (1997). Potential signalling roles for UTP and UDP: sources, regulation and release of uracil nucleotides. *Trends Pharmacol. Sci.* **18**, 387–392.
- Arendt, D. (2005). Genes and homology in nervous system evolution: comparing gene functions, expression patterns, and cell type molecular fingerprints. *Theory Biosci.* **124**, 185–197.
- Baye, L. M. and Link, B. A. (2007). Interkinetic nuclear migration and the selection of neurogenic cell divisions during vertebrate retinogenesis. *J. Neurosci.* **27**, 10143–10152.
- Bradford, Y., Conlin, T., Dunn, N., Fashena, D., Frazer, K., Howe, D. G., Knight, J., Mani, P., Martin, R., Moxon, S. A. et al. (2011). ZFIN: enhancements and updates to the Zebrafish Model Organism Database. *Nucleic Acids Res.* **39**, D822–D829.
- Brombin, A., Grossier, J. P., Heuzé, A., Radev, Z., Bourrat, F., Joly, J. S. and Jamen, F. (2011). Genome-wide analysis of the POU genes in medaka, focusing on expression in the optic tectum. *Dev. Dyn.* **240**, 2354–2363.
- Bugner, V., Tecza, A., Gessert, S. and Kühl, M. (2011). Peter Pan functions independently of its role in ribosome biogenesis during early eye and craniofacial cartilage development in *Xenopus laevis*. *Development* **138**, 2369–2378.

- Candal, E., Thermes, V., Joly, J. S. and Bourrat, F. (2004). Medaka as a model system for the characterisation of cell cycle regulators: a functional analysis of Ol-Gadd45gamma during early embryogenesis. *Mech. Dev.* **121**, 945-958.
- Candal, E., Alunni, A., Thermes, V., Jamen, F., Joly, J. S. and Bourrat, F. (2007). Ol-insm1b, a SNAG family transcription factor involved in cell cycle arrest during medaka development. *Dev. Biol.* **309**, 1-17.
- Cerveny, K. L., Varga, M. and Wilson, S. W. (2012). Continued growth and circuit building in the anamniote visual system. *Dev. Neurobiol.* **72**, 328-345.
- Chapouton, P., Adolf, B., Leucht, C., Tannhäuser, B., Ryu, S., Driever, W. and Bally-Cuif, L. (2006). her5 expression reveals a pool of neural stem cells in the adult zebrafish midbrain. *Development* **133**, 4293-4303.
- Chojnacki, A. K., Mak, G. K. and Weiss, S. (2009). Identity crisis for adult periventricular neural stem cells: subventricular zone astrocytes, ependymal cells or both? *Nat. Rev. Neurosci.* **10**, 153-163.
- Conesa, A., Götz, S., García-Gómez, J. M., Terol, J., Talón, M. and Robles, M. (2005). Blast2GO: a universal tool for annotation, visualization and analysis in functional genomics research. *Bioinformatics* **21**, 3674-3676.
- Devès, M. and Bourrat, F. (2012). Transcriptional mechanisms of developmental cell cycle arrest: problems and models. *Semin. Cell Dev. Biol.* **23**, 290-297.
- Efroni, S., Duttugupta, R., Cheng, J., Dehghani, H., Hoepfner, D. J., Dash, C., Bazett-Jones, D. P., Le Grice, S., McKay, R. D., Buetow, K. H. et al. (2008). Global transcription in pluripotent embryonic stem cells. *Cell Stem Cell* **2**, 437-447.
- England, S. J., Blanchard, G. B., Mahadevan, L. and Adams, R. J. (2006). A dynamic fate map of the forebrain shows how vertebrate eyes form and explains two causes of cyclopia. *Development* **133**, 4613-4617.
- Fichelson, P., Moch, C., Ivanovitch, K., Martin, C., Sidor, C. M., Lepesant, J. A., Bellaiche, Y. and Huynh, J. R. (2009). Live-imaging of single stem cells within their niche reveals that a U3snoRNP component segregates asymmetrically and is required for self-renewal in Drosophila. *Nat. Cell Biol.* **11**, 685-693.
- Fuchs, E., Tumber, T. and Guasch, G. (2004). Socializing with the neighbors: stem cells and their niche. *Cell* **116**, 769-778.
- Geldmacher-Voss, B., Reugels, A. M., Pauls, S. and Campos-Ortega, J. A. (2003). A 90-degree rotation of the mitotic spindle changes the orientation of mitoses of zebrafish neuroepithelial cells. *Development* **130**, 3767-3780.
- Götz, M. and Huttner, W. B. (2005). The cell biology of neurogenesis. *Nat. Rev. Mol. Cell Biol.* **6**, 777-788.
- Grandel, H. and Brand, M. (2013). Comparative aspects of adult neural stem cell activity in vertebrates. *Dev. Genes Evol.* **223**, 131-147.
- Grandel, H., Kaslin, J., Ganz, J., Wenzel, I. and Brand, M. (2006). Neural stem cells and neurogenesis in the adult zebrafish brain: origin, proliferation dynamics, migration and cell fate. *Dev. Biol.* **295**, 263-277.
- Greiling, T. M., Aose, M. and Clark, J. I. (2010). Cell fate and differentiation of the developing ocular lens. *Invest. Ophthalmol. Vis. Sci.* **51**, 1540-1546.
- Herbomel, P. (1999). Spinning nuclei in the brain of the zebrafish embryo. *Curr. Biol.* **9**, R627-R628.
- Hölzel, M., Rohrmoser, M., Schlee, M., Grimm, T., Harasim, T., Malamoussi, A., Gruber-Eber, A., Kremmer, E., Hiddemann, W., Bornkamm, G. W. et al. (2005). Mammalian WDR12 is a novel member of the Pes1-Bop1 complex and is required for ribosome biogenesis and cell proliferation. *J. Cell Biol.* **170**, 367-378.
- Hsieh, J. (2012). Orchestrating transcriptional control of adult neurogenesis. *Genes Dev.* **26**, 1010-1021.
- Ito, Y., Tanaka, H., Okamoto, H. and Ohshima, T. (2010). Characterization of neural stem cells and their progeny in the adult zebrafish optic tectum. *Dev. Biol.* **342**, 26-38.
- Kimmel, C. B., Ballard, W. W., Kimmel, S. R., Ullmann, B. and Schilling, T. F. (1995). Stages of embryonic development of the zebrafish. *Dev. Dyn.* **203**, 253-310.
- Kizil, C., Kaslin, J., Kroehne, V. and Brand, M. (2011). Adult neurogenesis and brain regeneration in zebrafish. *Dev. Neurobiol.* **72**, 429-461.
- Komili, S., Farny, N. G., Roth, F. P. and Silver, P. A. (2007). Functional specificity among ribosomal proteins regulates gene expression. *Cell* **131**, 557-571.
- Kondrashov, N., Pusic, A., Stumpf, C. R., Shimizu, K., Hsieh, A. C., Xue, S., Ishijima, J., Shiroishi, T. and Barna, M. (2011). Ribosome-mediated specificity in Hox mRNA translation and vertebrate tissue patterning. *Cell* **145**, 383-397.
- Koudijs, M. J., den Broeder, M. J., Keijser, A., Wienholds, E., Houwing, S., van Rooijen, E. M., Geisler, R. and van Eeden, F. J. (2005). The zebrafish mutants dre, ukl, and lep encode negative regulators of the hedgehog signaling pathway. *PLoS Genet.* **1**, e19.
- Kriegstein, A. and Alvarez-Buylla, A. (2009). The glial nature of embryonic and adult neural stem cells. *Annu. Rev. Neurosci.* **32**, 149-184.
- Kwan, K. M., Otsuna, H., Kidokoro, H., Carney, K. R., Saijoh, Y. and Chien, C. B. (2012). A complex choreography of cell movements shapes the vertebrate eye. *Development* **139**, 359-372.
- Law, J. A. and Jacobsen, S. E. (2010). Establishing, maintaining and modifying DNA methylation patterns in plants and animals. *Nat. Rev. Genet.* **11**, 204-220.
- Le Boutellier M., Souilhol C., Beck-Cormier S., Stedman A., Buren-Defranoux O., Vandormael-Pournin S., Bernex F., Cumano A. and Cohen-Tannoudji M. (2013). Notchless-dependent ribosome synthesis is required for the maintenance of adult hematopoietic stem cells. *J. Exp. Med.* **210**, 2351-2369.
- Link, B. A., Kainz, P. M., Ryou, T. and Dowling, J. E. (2001). The perplexed and confused mutations affect distinct stages during the transition from proliferating to post-mitotic cells within the zebrafish retina. *Dev. Biol.* **236**, 436-453.
- Liu, Y. C., Li, F., Handler, J., Huang, C. R., Xiang, Y., Neretti, N., Sedivy, J. M., Zeller, K. I. and Dang, C. V. (2008). Global regulation of nucleotide biosynthetic genes by c-Myc. *PLoS ONE* **3**, e2722.
- Locker, M., Agathocleous, M., Amato, M. A., Parain, K., Harris, W. A. and Perron, M. (2006). Hedgehog signaling and the retina: insights into the mechanisms controlling the proliferative properties of neural precursors. *Genes Dev.* **20**, 3036-3048.
- Mathis, L. and Nicolas, J. F. (2006). Clonal origin of the mammalian forebrain from widespread oriented mixing of early regionalized neuroepithelium precursors. *Dev. Biol.* **293**, 53-63.
- Mishra, S., Murphy, L. C. and Murphy, L. J. (2006). The Prohibitins: emerging roles in diverse functions. *J. Cell. Mol. Med.* **10**, 353-363.
- Müller, F. J., Laurent, L. C., Kostka, D., Ulitsky, I., Williams, R., Lu, C., Park, I. H., Rao, M. S., Shamir, R., Schwartz, P. H. et al. (2008). Regulatory networks define phenotypic classes of human stem cell lines. *Nature* **455**, 401-405.
- Neumüller, R. A., Richter, C., Fischer, A., Novatchkova, M., Neumüller, K. G. and Knoblich, J. A. (2011). Genome-wide analysis of self-renewal in Drosophila neural stem cells by transgenic RNAi. *Cell Stem Cell* **8**, 580-593.
- Olivier, N., Luengo-Oroz, M. A., Duloquin, L., Faure, E., Savy, T., Veilleux, I., Solinas, X., Débarre, D., Bourguin, P., Santos, A. et al. (2010). Cell lineage reconstruction of early zebrafish embryos using label-free nonlinear microscopy. *Science* **329**, 967-971.
- Palmgren, A. (1921). Embryological and morphological studies on the mid-brain and cerebellum of vertebrates. *Acta Zoologica* **2**, 1-94.
- Parain, K., Mazurier, N., Bronchain, O., Borden, C., Cabochette, P., Chesneau, A., Colozza, G., El Yakoubi, W., Hamdache, J., Locker, M. et al. (2011). A large scale screen for neural stem cell markers in Xenopus retina. *Dev. Neurobiol.* **72**, 491-506.
- Perrera, C., Colombo, R., Valsasina, B., Carpinelli, P., Troiani, S., Modugno, M., Gianellini, L., Cappella, P., Isacchi, A., Moll, J. et al. (2010). Identification of Myb-binding protein 1A (MYBBP1A) as a novel substrate for aurora B kinase. *J. Biol. Chem.* **285**, 11775-11785.
- Peyre, E., Jaouen, F., Saadaoui, M., Haren, L., Merdes, A., Durbec, P. and Morin, X. (2011). A lateral belt of cortical LGN and NuMA guides mitotic spindle movements and planar division in neuroepithelial cells. *J. Cell Biol.* **193**, 141-154.
- Ramialison, M., Reinhardt, R., Henrich, T., Wittbrodt, B., Kellner, T., Lowy, C. M. and Wittbrodt, J. (2012). Cis-regulatory properties of medaka synexpression groups. *Development* **139**, 917-928.
- Rieger, S., Wang, F. and Sagasti, A. (2011). Time-lapse imaging of neural development: zebrafish lead the way into the fourth dimension. *Genesis* **49**, 534-545.
- Rinkwitz, S., Mourrain, P. and Becker, T. S. (2011). Zebrafish: an integrative system for neurogenomics and neurosciences. *Prog. Neurobiol.* **93**, 231-243.
- Rothenaigier, I., Krecsmarik, M., Hayes, J. A., Bahn, B., Lepier, A., Fortin, G., Götz, M., Jagasia, R. and Bally-Cuif, L. (2011). Clonal analysis by distinct viral vectors identifies bona fide neural stem cells in the adult zebrafish telencephalon and characterizes their division properties and fate. *Development* **138**, 1459-1469.
- Ruggero, D. and Pandolfi, P. P. (2003). Does the ribosome translate cancer? *Nat. Rev. Cancer* **3**, 179-192.
- Schmidt, R., Strähle, U. and Scholpp, S. (2013). Neurogenesis in zebrafish - from embryo to adult. *Neural Dev.* **8**, 3.
- Sheng, J., Yang, S., Xu, L., Wu, C., Wu, X., Li, A., Yu, Y., Ni, H., Fukuda, M. and Zhou, J. (2004). Bystin as a novel marker for reactive astrocytes in the adult rat brain following injury. *Eur. J. Neurosci.* **20**, 873-884.
- Sigoillot, F. D., Evans, D. R. and Guy, H. I. (2002). Growth-dependent regulation of mammalian pyrimidine biosynthesis by the protein kinase A and MAPK signaling cascades. *J. Biol. Chem.* **277**, 15745-15751.
- Solnica-Krezel, L., Schier, A. F. and Driever, W. (1994). Efficient recovery of ENU-induced mutations from the zebrafish germline. *Genetics* **136**, 1401-1420.
- Steinmetz, P. R., Kostyuchenko, R. P., Fischer, A. and Arendt, D. (2011). The segmental pattern of otx, gbx, and Hox genes in the annelid Platynereis dumerilii. *Evol. Dev.* **13**, 72-79.
- Subramanian, A., Tamayo, P., Mootha, V. K., Mukherjee, S., Ebert, B. L., Gillette, M. A., Paulovich, A., Pomeroy, S. L., Golub, T. R., Lander, E. S. et al. (2005). Gene set enrichment analysis: a knowledge-based approach for interpreting genome-wide expression profiles. *Proc. Natl. Acad. Sci. USA* **102**, 15545-15550.
- Tsuchiya, M., Katagiri, N., Kuroda, T., Kishimoto, H., Nishimura, K., Kumazawa, T., Iwasaki, N., Kimura, K. and Yanagisawa, J. (2011). Critical role of the nucleolus in activation of the p53-dependent postmitotic checkpoint. *Biochem. Biophys. Res. Commun.* **407**, 378-382.
- Willer, G. B., Lee, V. M., Gregg, R. G. and Link, B. A. (2005). Analysis of the Zebrafish perplexed mutation reveals tissue-specific roles for de novo pyrimidine synthesis during development. *Genetics* **170**, 1827-1837.
- Xu, Q., Holder, N., Patient, R. and Wilson, S. W. (1994). Spatially regulated expression of three receptor tyrosine kinase genes during gastrulation in the zebrafish. *Development* **120**, 287-299.
- Xue, X. Y. and Harris, W. A. (2011). Using myc genes to search for stem cells in the ciliary margin of the Xenopus retina. *Dev. Neurobiol.* **72**, 475-490.
- Zhang, Y., Duc, A. C., Rao, S., Sun, X. L., Bilbee, A. N., Rhodes, M., Li, Q., Kappes, D. J., Rhodes, J. and Wiest, D. L. (2013). Control of hematopoietic stem cell emergence by antagonistic functions of ribosomal protein paralogs. *Dev. Cell* **24**, 411-425.
- Zhao, C., Deng, W. and Gage, F. H. (2008). Mechanisms and functional implications of adult neurogenesis. *Cell* **132**, 645-660.
- Zupanc, G. K. (2009). Towards brain repair: Insights from teleost fish. *Semin. Cell Dev. Biol.* **20**, 683-690.
- Zupanc, G. K. and Sîrbulescu, R. F. (2011). Adult neurogenesis and neuronal regeneration in the central nervous system of teleost fish. *Eur. J. Neurosci.* **34**, 917-929.

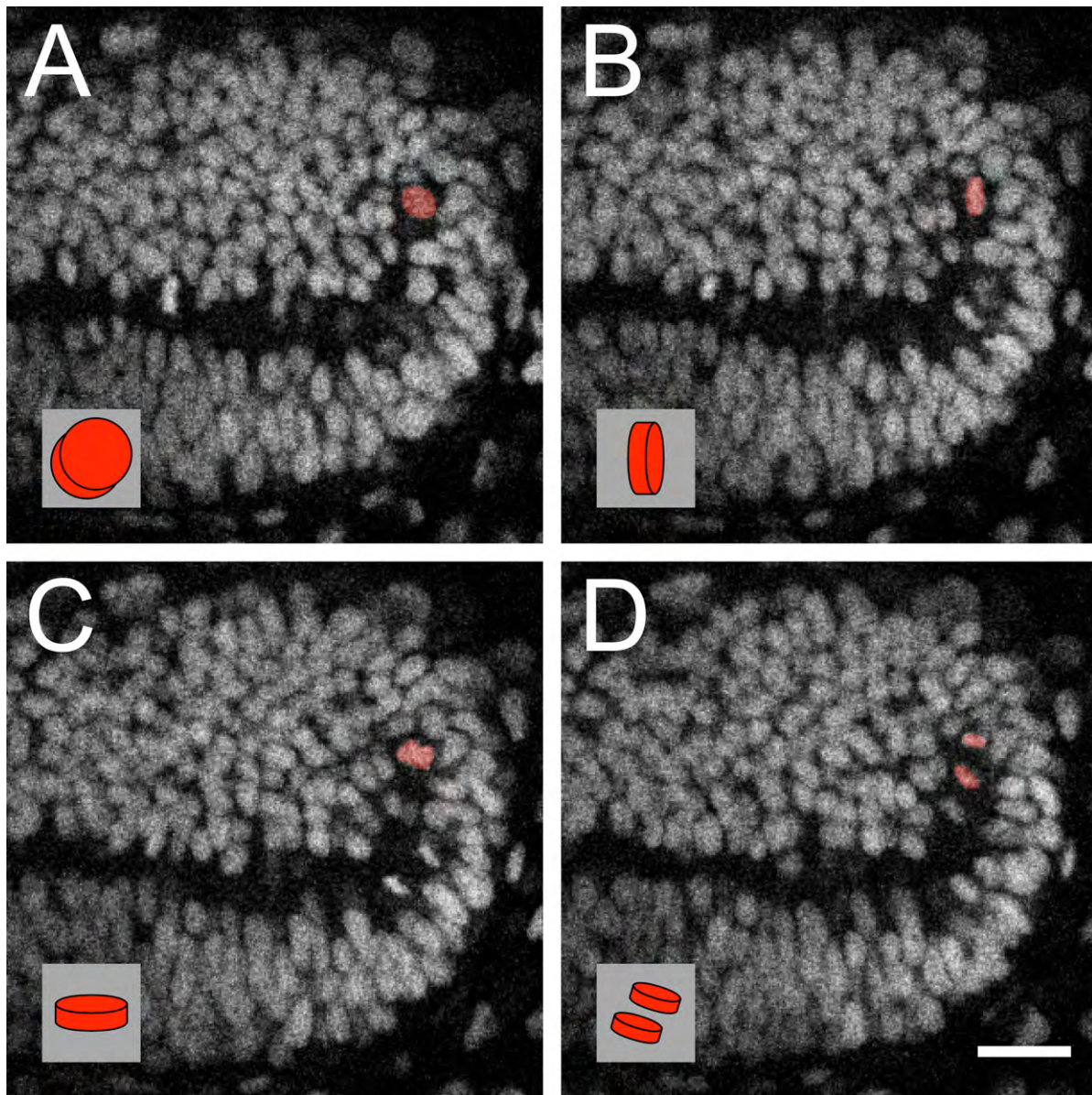


Fig. S1. Metaphase plate rotation prior to mitosis

The metaphase plate is initially in the plane of imaging, then perpendicular to image plane, parallel to the PML and finally turns perpendicular to the PML, resulting in a planar radial division.

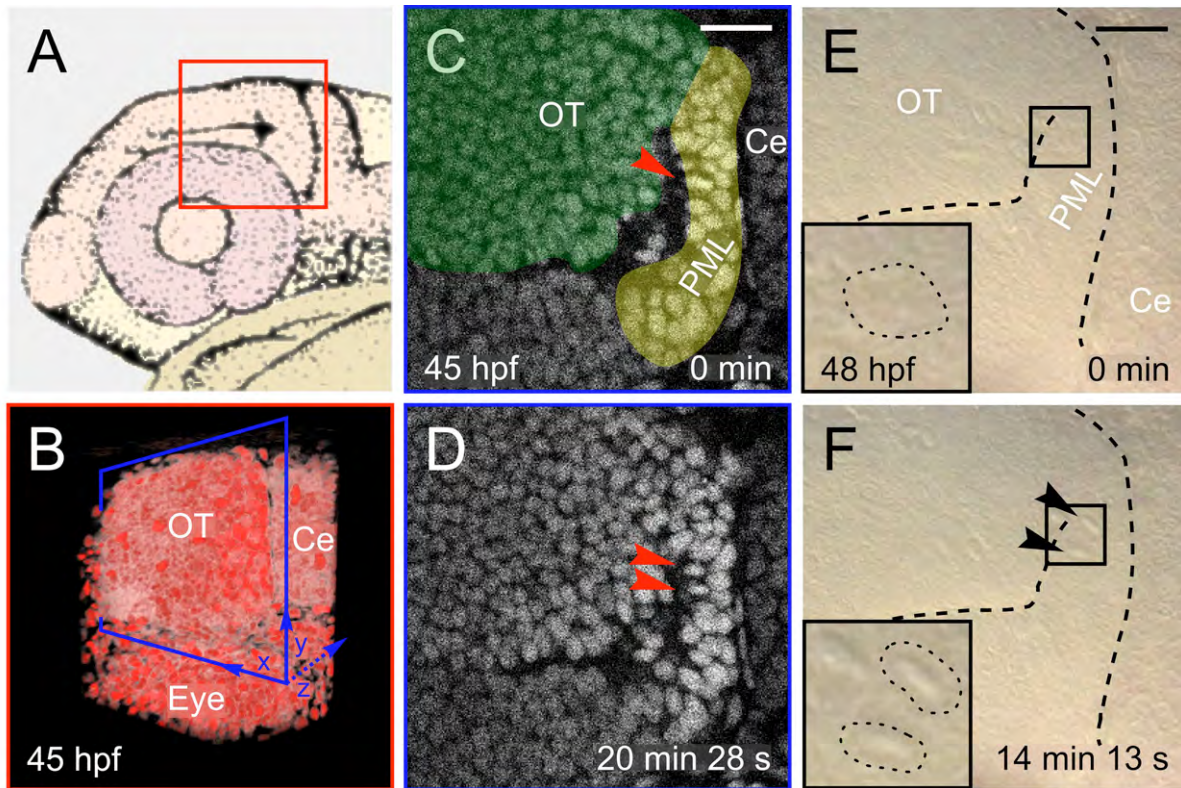


Fig. S2. TPLSM imaging: orientation and non-invasiveness

(A) Schematic drawing of a 31 hpf (prim-16) zebrafish larva head (adapted from (Kimmel et al., 1995)). Fish were mounted laterally so as to have access to the lateral side of the brain with a dipping lens objective. Red square: field of view imaged in (B).

(B) 3D rendering (obtained with Mov-IT) of the imaged field at 45 hpf. Anterior part is on the left and dorsal side on the top. OT: optic tectum; Ce: cerebellum. Blue square: sagittal optical sections in (C) and (D).

(C-F) Location and timing of mitoses in the PML for transgenic fish (TPLSM imaging, C-D) and WT fish (Nomarski imaging [Nikon DXM 1200 camera on Zeiss SV11 (Herbomel, 1999)], E-F). Prophase (C-E) and telophase (D-F) stages of a mitosis (arrow heads). Scale bars: 20 μ m.

Fig. S3 (linked to Fig. 4). Pattern of PML and proliferation genes extracted from ZFIN

(A) Expression pattern of *cdc20* as an example of genes expressed in all proliferation zones of the anterior nervous system. (B) Expression patterns of the thinly expressed PML-specific gene *cad* at early stages (1–4 somites to 10–13 somites, 14–19 somites and 20–25 somites to prim-5). (C) Expression pattern of the PML-specific gene *nop58* at prim-15 to prim-25 stages (C_{1-2}) and at high-primitive/long-primitive stages (C_{1-2}). (D-Z; AA-ZZ) Expression patterns of 49 PML genes (in blue frame), (AAA-ZZZ; AAAAA-ZZZZ; AAAAAA-PPPPP) Expression patterns of 68 proliferation genes (in red frame). Stages and views are indicated at the top of each picture. In each line, the first and second pictures show ISH expression pattern in a 15–25 embryo (36 hr - 36 hpf) in dorsal and lateral views, respectively. The third picture shows the corresponding whole-mount view.

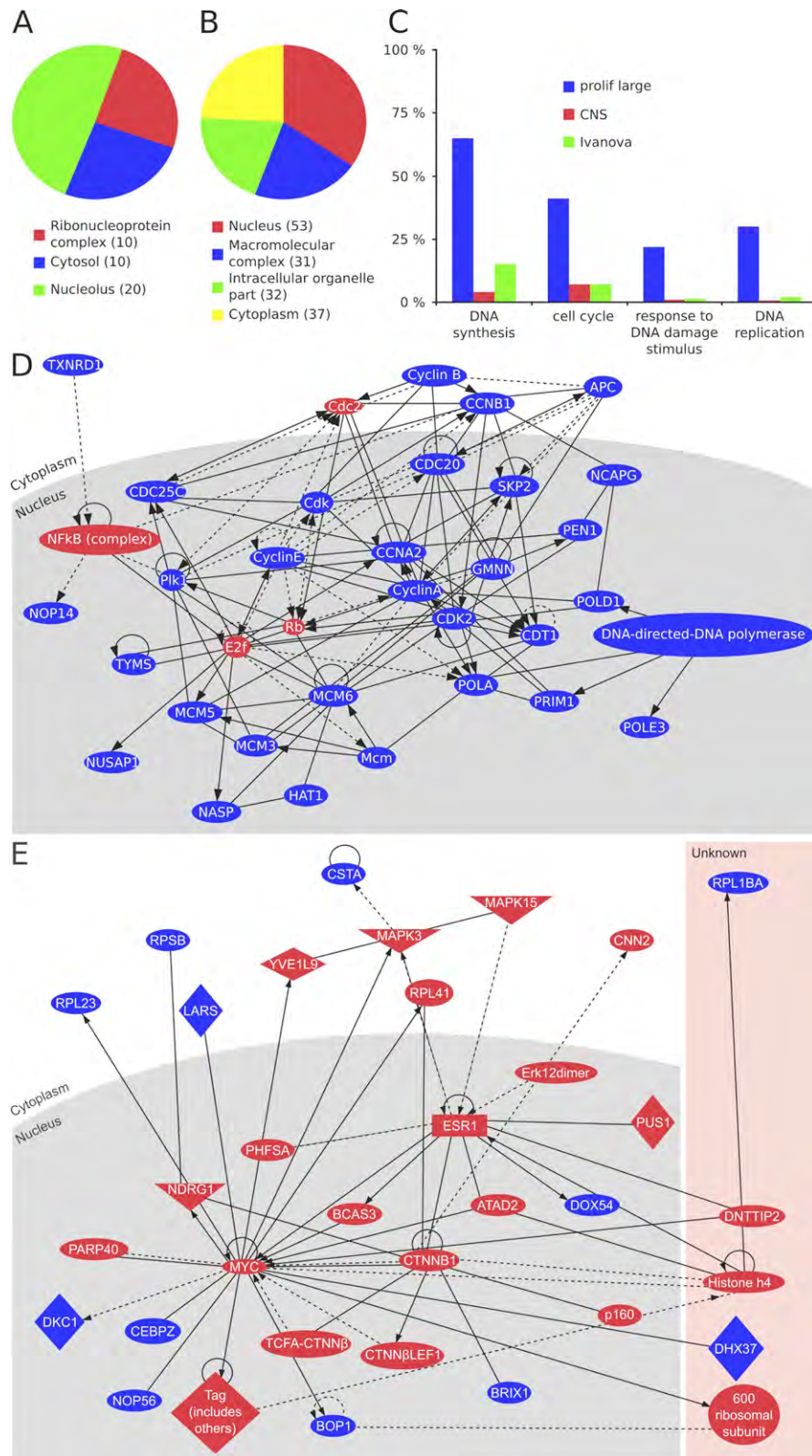
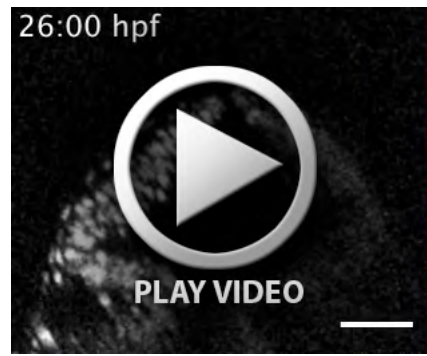
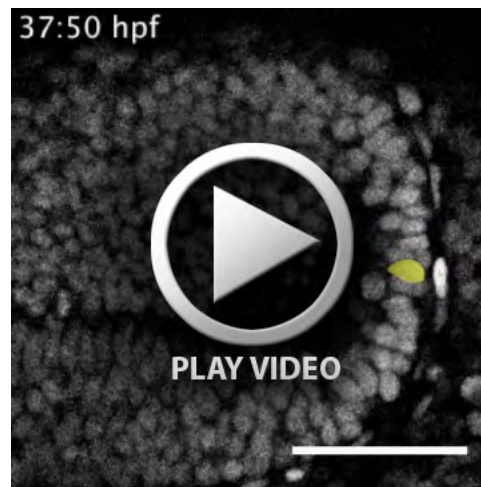


Fig. S4 The highly interconnected network of proliferation genes and the *Drosophila* neuroblast gene network

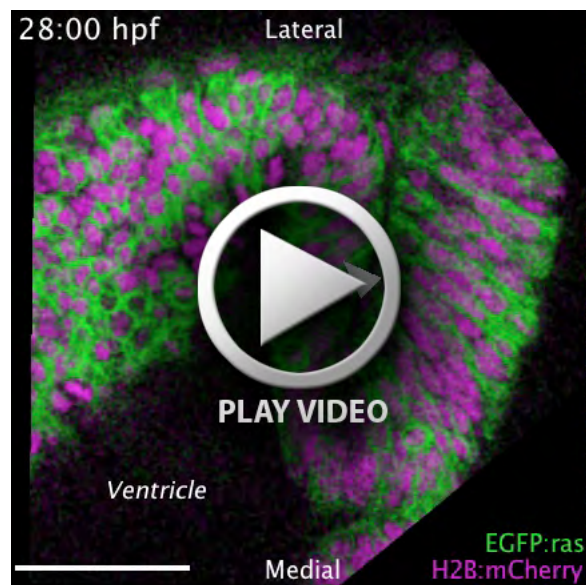
(A, B) Blast2GO cellular component term analysis (A) A multilevel pie chart (cut-off = 10) for the PML-specific genes showing a large proportion of their products are active in the nucleolus. (B) A multilevel pie chart (cut-off = 30) for the group of genes with wide expression patterns showing that a large proportion of their products are active in the nucleus. (C) Histograms illustrating the comparative results of GO enrichment analysis (Fisher's Exact Test) for the list of genes with wide expression pattern (using the lists of CNS genes, and of Ivanova Hematopoiesis Mature Cells (HMC) genes, as backgrounds). (D) Ingenuity® pathway analysis networks for the dataset of genes with a wide expression pattern. (E) The main *Drosophila* neuroblast network is interconnected with the fish network and contains nucleolar and ribosomal proteins (Neumuller et al., 2011).



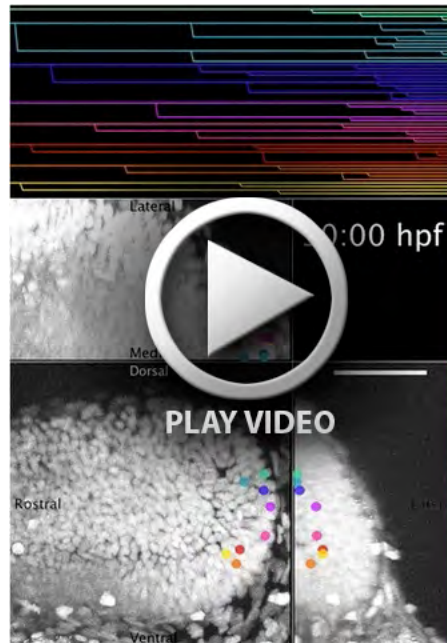
Movie 1 (linked to Fig. 1). Morphogenesis of the midbrain from 26:00 hpf to 46:00 hpf. Transversal section, H2B:Venus. Scale bar: 50 μ m.



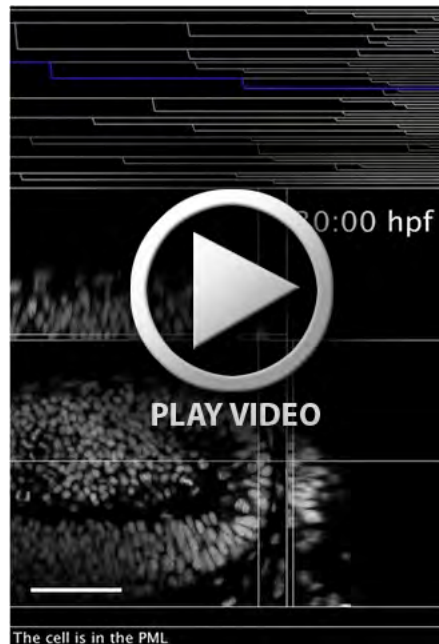
Movie 2 (linked to Fig. 2). Mitoses in the PML (yellow) and in the OT (green). Parasagittal section, H2B:Venus. Scale bar: 50 μ m.



Movie 3 (linked to Fig. 2). Interkinetic migration in the PML. Horizontal section, H2B:mCherry, EGFP:ras. Scale bar: 50 μ m.



Movie 4 (linked to Fig. 3). Cell-tracking of eight clones from the PML to the OT with time course shown on the lineage trees. Trajectories are represented overlaid with the maximal projection of the volume, on the top image: top view projection, on the main image: lateral view projection and on the right image: frontal view projection.



Movie 5 (linked to Fig. 3). Example of typical clone behaviour from the PML to the OT. The blue cell is followed from the PML to the OT. Location of the cell is indicated by the intersection of the lines on each section (top image: horizontal section, main image: parasagittal section and right image: transverse section). Mitosis occurrences and cell location are made explicit in the bottom lines.



Movie 6 (linked to Fig. 3). Example of a clone that give rise to cells located both in the OT and in the TS. At the beginning of the movie, both panels are identical until mitoses occurs, then cells follow their own way, the left one going down the TS and the right one going up the OT, as indicated by the lines that locate either below or upon the ventricle lumen.

Table S1. List of NSC, proliferation and other genes

Data provided from Muller et al. [PluriNet (Muller et al., 2008)], Yan Jaszczyszyn (CNS list, personal communication), Neumuller [Drosophila neuroblasts (Neumuller et al., 2011)] and MSigDB v3.0 (Ivanova Hematopoiesis Mature Cells list (<http://www.broadinstitute.org/gsea/msigdb/index.jsp>))]

Table S2. List of the 20 first hits in the MSig analysis. Most are found on cancer lists.

Table S3. Phenotypes of zebrafish mutants for PML-expressed genes

There are mutant alleles available for 18 of the 51 “thinly” expressed PML genes (36%). Almost all of them have been generated via insertional mutagenesis (Amsterdam et al., 1999). The *cad⁵²* allele is the only one obtained by ENU-mediated mutagenesis (Solnica-Krezel et al., 1994). Mutant homozygote embryos of the different lines share common phenotypes and almost all of them display smaller head and eyes (HE) if compared to wild-type embryos; vertebrate retinal development, and neurogenesis in general, can be viewed as a sequence of coordinated events. Shared phenotypes include several defects in the development of neuroectodermal derivatives. In most cases, mutant embryos show different levels of CNS cells necrosis (CNS), a pinched midbrain/hindbrain boundary (MHB) and an inflated hindbrain ventricle (IHV). Thinly expressed PML genes encode for ubiquitous proteins participating in pathways such as those for ribosome biogenesis and pyrimidine/purine biosynthesis. Other phenotypes, such as the presence of a pericardial oedema (PO) and underdevelopment of the liver/gut (LG), are often accompanied by an unabsorbed yolk (round grey yolk, RY). All the phenotypes described could be seen between the second and the fifth day of development. Less is known about mutant embryos at later developmental stages. CNSn: Central Nervous System necrosis; HE: smaller head and eyes; IHV: inflated hindbrain ventricle; LG: underdeveloped liver/gut; MHB: pinched midbrain/hindbrain boundary; RY: rounder grey yolk.

Table S4. List of probes used for ISH

Plurinet list (<i>Homo sapiens</i>)		Proliferation zones list (<i>Danio rerio</i>)		PML list (<i>Danio rerio</i>)		CNS list (control) <i>Danio rerio</i>		Neuroblast- associated genes involved in ribosome biogenesis (<i>Drosophila melanogaster</i>)		Orthologues (<i>Mus musculus</i>)		IVANOVA hematopoiesis mature cell list (<i>Mus musculus</i>)
AATF	ENSG00000108270	Ahcy	ENSDARG00000005191	adi1	ENSDARG00000020448	ahcY	ENSDARG00000005191	cdc16	FBgn0025781			1100001G20RIK
ACTA1	ENSG00000143632	anp32b	ENSDARG00000023330	atic	ENSDARG00000016706	ak5l	ENSDARG00000017739	Cdc27	FBgn0012058			1110038D17RIK
ANAPC1	ENSG00000153107	asc11a	ENSDARG00000038386	Bxdc1 (rpf2)	ENSDARG00000043960	aldh2a	ENSDARG00000028087	CG11180	FBgn0034528	Pinx1		1500003O03RIK
ANP32A	ENSG00000140350	ccna2	ENSDARG00000011094	Bysl	ENSDARG00000001057	aldh2b	ENSDARG00000028087	CG11583	FBgn0035524	bxdc2		1810037117RIK
ANXA2	ENSG00000182718	ccnb1	ENSDARG00000051923	cad	ENSDARG00000041895	alp	ENSDARG00000015546	CG12325	FBgn0033557	pwp2		1810058124RIK
anxa3	ENSG00000138772	ccnd1	ENSDARG00000035750	cnbp (zff9)	ENSDARG00000045776	anp32b	ENSDARG00000023330	CG1671	FBgn0033454	tbl3		2310035K24RIK
Apex1	ENSG00000100823	ccne2	ENSDARG00000027918	ctps	ENSDARG00000030700	arhgap29b	ENSDARG00000017748	CG1785	FBgn0030061	gltscr2		2810453I06RIK
APOE	ENSG00000130203	ccnf	ENSDARG00000034763	Ddx18	ENSDARG00000030789	arl31	ENSDARG00000028846	CG32344	FBgn0052344	ddx54		2810453I06RIK
Arid3b	ENSG00000179361	Cdc20	ENSDARG00000020192	dnmt4	ENSDARG00000036791	arr3l	ENSDARG00000056511	CG33123	FBgn0053123	lars		ACP1
ARL4A	ENSG00000122644	Cdc25	ENSDARG00000010792	ect2	ENSDARG00000007278	ARX	ENSDARG00000058011	CG4554	FBgn0034734	Utp20		ACP5
Armc6	ENSG00000105676	cdca7	ENSDARG00000077620	Fbl	ENSDARG00000053912	atoh2b	ENSDARG00000020794	CG4806	FBgn0035048	rbm28		ACSL1
ATIC	ENSG00000138363	Cdca8	ENSDARG00000043137	fpgs	ENSDARG00000044809	atp1b1a	ENSDARG00000013144	CG5033	FBgn0028744	BOP1		ACTA2
AURKA	ENSG00000087586	cdk2	ENSDARG00000026577	ftsj	ENSDARG00000076761	AURKB	ENSDARG00000037640	CG5317	FBgn0032404	RpL7I		ADD1
AURKB	ENSG00000178999	cdt1	ENSDARG00000051854	gart	ENSDARG00000051855	BARHL2	ENSDARG00000070129	CG5800	FBgn0030855	ddx10		AGFG1
Bak1	ENSG00000030110	chaf1a	ENSDARG00000062152	hells	ENSDARG00000057738	BCAT1	ENSDARG00000045568	CG7338	FBgn0037073	tsr1		ALAS2
bat3	ENSG00000204463	Chtf18	ENSDARG00000058480	imp4	ENSDARG00000054540	BHLHE23	ENSDARG00000037588	CG7728	FBgn0036686	bms1		AMPD3
bccip	ENSG00000107949	cldn5a	ENSDARG00000043716	impdh2	ENSDARG00000006900	c3orf58a	ENSDARG00000012816	CG7839	FBgn0036124	Cebpz		ANKRD43
BCL2	ENSG00000171791	Cx43.4	ENSDARG0000007099	kars	ENSDARG00000044220	calrl2	ENSDARG00000076290	CG7993	FBgn0038585	bxdc1		ARL2BP
BIK	ENSG00000100290	Ddx27	ENSDARG00000091831	lars	ENSDARG00000019280	cdx4	ENSDARG00000036292	CG8064	FBgn0038597	wdr3		ASNS
BIRC5	ENSG00000089685	dlc	ENSDARG00000002336	metap1	ENSDARG00000033440	col7a1l	ENSDARG00000069692	CG8461	FBgn0038235	rrp36		ATP6V1E1
Blm	ENSG00000197299	dnmt1	ENSDARG00000030756	mki67ip	ENSDARG00000040666	csrp1a	ENSDARG00000006603	CG9246	FBgn0032925	noc3l		BMP2K
BTBD14B	ENSG00000160877	Dscc1	ENSDARG00000019907	Mybbp1a	ENSDARG00000078214	dlx1a	ENSDARG00000013125	Dbp73D	FBgn0004556			BNIP3L
BUB1B	ENSG00000156970	Dut	ENSDARG00000086768	Myca	ENSDARG00000045695	dlx2a	ENSDARG00000079964	eIF-4E	FBgn0015218			C1QB
BXDC2	ENSG00000113460	fen1	ENSDARG00000011404	nap1l4a	ENSDARG00000070560	dlx5a	ENSDARG00000042296	Hlc	FBgn0001565			C3
bysl	ENSG00000112578	Gmnn	ENSDARG00000035957	nat10	ENSDARG00000054259	dmbx1b	ENSDARG00000002510	ida	FBgn0041147			CCDC142
C1orf103	ENSG00000121931	Hat1	ENSDARG00000034916	nle1	ENSDARG00000057105	efna2	ENSDARG00000031372	kz	FBgn0001330			CCNA2
C8orf32	ENSG00000156795	Hn1l	ENSDARG00000034427	noc3l	ENSDARG00000002487	efna5a	ENSDARG00000057223	lp259	FBgn0025366			CCRN4L
CASP6	ENSG00000138794	ipo9	ENSDARG00000016753	noc4l	ENSDARG00000045565	Egfl6	ENSDARG00000045958	Mys45A	FBgn0033379			CD14
Casp9	ENSG00000132906	Kpna2	ENSDARG00000038066	nop56	ENSDARG00000012820	egr2b	ENSDARG00000042826	Nmd3	FBgn0023542			CDAC3
CCDC5	ENSG00000152240	Mat2a	ENSDARG00000040334	nop58	ENSDARG00000058337	elovl4b	ENSDARG00000027495	Nop56	FBgn0038964			CDK8
CCNA2	ENSG00000145386	Mcm3	ENSDARG00000024204	npm1 (npm1a)	ENSDARG00000014329	EMX1	ENSDARG00000039569	Nop60B	FBgn0023184			CDKN2D
CCNB1	ENSG00000134057	Mcm5	ENSDARG00000019507	pcca	ENSDARG00000028982	emx2	ENSDARG00000039701	Rpl135	FBgn0003278			CDKN3
CCNB2	ENSG00000157456	Mcm6	ENSDARG00000057683	pccb	ENSDARG00000038910	emx3	ENSDARG00000020417	Rpl10Aa	FBgn0038281			CDR2
CCND1	ENSG00000110092	msh2	ENSDARG00000018022	Pdcd11	ENSDARG00000052480	eomesa	ENSDARG00000006640	Rpl23	FBgn0010078			CELA1
CCNE1	ENSG00000105173	Msh6	ENSDARG00000011666	pes	ENSDARG00000018902	EVX1	ENSDARG00000005628	RpS10a	FBgn0027494			CES3
cda	ENSG00000158825	Msi1	ENSDARG00000010710	phb	ENSDARG00000057414	FEZF2	ENSDARG00000070677	RpS29	FBgn0037752			CMAS
CDC2	ENSG00000170312	Nasp	ENSDARG00000039208	pno1	ENSDARG00000008502	FGF22	ENSDARG00000076510	RpS8	FBgn0039713			COL1A1
CDC25C	ENSG00000158402	ncapd2	ENSDARG00000005058	Polr1b	ENSDARG00000077469	foxg1a	ENSDARG00000070769	shtd	FBgn0004391			CTSB
Cdc45	ENSG00000093009	ncapg	ENSDARG00000070109	Ppan	ENSDARG00000022232	foxg1b	ENSDARG00000032705					CTSH
CDC7	ENSG00000097046	Nop14	ENSDARG00000033945	ppat	ENSDARG00000004517	foxh1	ENSDARG00000055630					CYBB
CDK7	ENSG00000134058	npepps	ENSDARG00000044943	pprc1	ENSDARG00000090337	fryb	ENSDARG00000056001					DCK
Cdt1	ENSG00000167513	Nusap1	ENSDARG00000002403	prdx3	ENSDARG00000032102	fut9	ENSDARG00000067524					DEGS1

Cebpz	ENSG00000115816	Parp2	ENSDARG00000079202	prps1a	ENSDARG00000015524	GBX1	ENSDARG00000071418	EAR1
CENPE	ENSG00000138778	Plk1	ENSDARG00000058471	rpl171	ENSDARG00000042864	glra4a	ENSDARG00000006885	EAR2
CHAF1A	ENSG00000167670	pola1	ENSDARG00000045308	rrp1	ENSDARG00000027515	HADHA	ENSDARG000000057128	EGFR
CHEK1	ENSG00000149554	Pold1	ENSDARG00000027689	rrp12	ENSDARG00000022410	hoxa2b	ENSDARG00000023031	EMR1
CHEK2	ENSG00000183765	pole3	ENSDARG00000008551	Shmt1	ENSDARG00000052816	hoxa3a	ENSDARG00000036231	EPOR
cks1b	ENSG00000173207	Ppm1g	ENSDARG00000075559	umps	ENSDARG00000012215	hoxa4a	ENSDARG00000057724	EPS15
CKS2	ENSG00000123975	Prim1	ENSDARG00000040163	wdr12	ENSDARG00000003287	hoxa5a	ENSDARG00000001784	FCNA
COIL	ENSG00000121058	psat1	ENSDARG00000016733	wdr46	ENSDARG000000095879	hoxa9a	ENSDARG00000009461	FPR1
Cops3	ENSG00000141030	Ptgr1	ENSDARG00000024877	wdr75	ENSDARG00000040730	hoxb1b	ENSDARG00000054033	FPR2
Cops6	ENSG00000168090	rars	ENSDARG00000054530			hoxb2a	ENSDARG00000000175	GADD45A
CROP	ENSG00000108848	rfc2	ENSDARG00000014274			hoxb5a	ENSDARG00000013057	GCNT1
CTBP2	ENSG00000175029	rfc4	ENSDARG00000042458			hoxb5b	ENSDARG00000054030	GOLIM4
cxadr	ENSG00000154639	Rpa3	ENSDARG00000002613			hoxb6a	ENSDARG00000010630	GP49A
DAXX	ENSG00000204209	Rrm1	ENSDARG00000014017			hoxb6b	ENSDARG00000026513	GPX4
DAZAP1	ENSG00000071626	Rrm2	ENSDARG00000020711			hoxb8a	ENSDARG00000056027	GPX4
DDX11	ENSG0000013573	Rrs1	ENSDARG00000003941			hoxc1a	ENSDARG00000070337	GRINA
DHCR24	ENSG00000116133	Skp2	ENSDARG00000004937			hoxc4a	ENSDARG00000070338	GTF2A1
DHFRL1	ENSG00000178700	smc2	ENSDARG00000017744			hoxc6a	ENSDARG00000070343	GTPBP2
DIAPH1	ENSG00000131504	smc4	ENSDARG00000038882			hoxc8a	ENSDARG00000070346	GYP A
DNMT3B	ENSG00000088305	Ssb	ENSDARG00000029252			hoxd3a	ENSDARG00000059280	H2-T24
dppA2	ENSG00000163530	tacc3	ENSDARG00000005454			hoxd4a	ENSDARG00000059276	HAGH
DSCC1	ENSG00000136982	Txnrd1	ENSDARG00000017864			hpvt11	ENSDARG00000014866	HBA-A1
ELAC2	ENSG00000006744	Txnrd3	AY221258 ZDB-GENE-030327-3	irx2a		igfbp1a	ENSDARG00000014947	HBA-A1
		tyms	ENSDARG00000042894				ENSDARG00000001785	HBB-B2
Erbb3	ENSG00000065361	xpo4	ENSDARG00000010281			irx6a	ENSDARG00000034420	HBB-B2
ERCC5	ENSG00000134899	xrcc6	ENSDARG00000071551			irx7	ENSDARG00000002601	HEBP1
EU176320	ENSG00000130332					kcnip1b	ENSDARG00000034808	HEMGN
EWSR1	ENSG00000182944					kif7l	ENSDARG000000043821	HGSNAT
Exo1	ENSG00000174371					lhx1a	ENSDARG00000018611	HIATL1
Exosc3	ENSG00000107371					lhx1b	ENSDARG00000018611	HIATL1
EXOSC7	ENSG00000075914					lft1	ENSDARG00000019920	HTATIP2
EXOSC8	ENSG00000120699					lhx1a	ENSDARG00000014018	ITGAM
EXOSC9	ENSG00000123737					lhx8a	ENSDARG00000002330	ITGB2L
FBL	ENSG00000105202					Lhx9	ENSDARG00000056979	KLF3
Fbp1	ENSG00000165140					LMO1	ENSDARG00000034504	LAMP2
FEN1	ENSG00000168496					mab2111	ENSDARG00000055089	LGMN
FKBP3	ENSG00000100442					Mab2112	ENSDARG00000015266	LILRB3
FLJ14668	ENSG00000035141					MMP23B	ENSDARG00000009825	LOC100045163
FOXO4	ENSG00000184481					MORN4	ENSDARG00000039062	LRG1
FUBP1	ENSG00000162613					MPPED2	ENSDARG00000034443	LY6G
fus	ENSG00000089280					MPZ	ENSDARG00000038609	MGST3
GADD45A	ENSG00000116717					neurod	ENSDARG00000019566	MKRN1
GDF9	ENSG00000164404					nkx2.1b	ENSDARG00000019835	MMP8
GEMIN6	ENSG00000152147					nkx2.2a	ENSDARG00000053298	MPP1
GEMIN7	ENSG00000142252					nkx2.2b	ENSDARG00000052550	MRC1
gmnn	ENSG00000112312					nkx2.9	ENSDARG00000020332	MRPL53
GMPS	ENSG00000163655					nkx6.2	ENSDARG00000044075	MTHFD2
gnl3	ENSG00000163938					nr2e1	ENSDARG00000017107	OTUD5
Got2	ENSG00000125166					nr5a1b	ENSDARG00000023362	PCX
GPRIN2	ENSG00000204175							

Grb7	ENSG00000141738	otpa	ENSDARG00000014201	PGLYRP1
Hdac1	ENSG00000116478	otpb	ENSDARG00000058379	PIGQ
HDAC2	ENSG00000196591	otx1a	ENSDARG00000030703	POOX
Hist1h2bc	ENSG00000180596	Otx2	ENSDARG00000011235	PPP3R1
HMGA1	ENSG00000137309	otx5	ENSDARG00000043483	PQLC3
HMGB1	ENSG00000189403	pax6a	ENSDARG00000045936	PRC1
HMMR	ENSG00000072571	pax6b	ENSDARG00000045936	RAB24
Hnrnpab	ENSG00000197451	prdm8	ENSDARG00000025017	RAB6
Hnrnpk	ENSG00000165119	prdm8b	ENSDARG00000054683	RBMS1
HPRT1	ENSG00000165704	rock2b	ENSDARG00000004877	RHAG
HSP90AB1	ENSG00000096384	rrp1	ENSDARG00000027515	RHD
HSPA14	ENSG00000187522	rtk8	ENSDARG00000027112	RNF141
Hspa2	ENSG00000126803	shox2	ENSDARG00000075713	RNF167
HSPA8	ENSG00000109971	si	ENSDARG00000075347	RNF19A
HSPA9	ENSG00000113013	six3a	ENSDARG00000058008	SCD1
HSPD1	ENSG00000144381	six3b	ENSDARG00000054879	SDCBP
HSPE1	ENSG00000115541	sncga	ENSDARG00000034423	SLC11A1
HSPH1	ENSG00000120694	ST8SIA2	ENSDARG00000018788	SLC16A1
ITGB3BP	ENSG00000142856	STC2	ENSDARG00000056680	SLC1A5
JTV1	ENSG00000106305	TBR1	ENSDARG00000004712	SLC4A1
KIT	ENSG00000157404	TBX20	ENSDARG00000005150	SLC7A8
KPNA2	ENSG00000182481	tpbgl	ENSDARG00000040216	SLFN3
KPNB1	ENSG00000108424	VAX1	ENSDARG00000021916	SLFN4
LCK	ENSG00000182866	wu	ENSDARG00000027515	SNCA
LOC728340	ENSG00000145736	zgc	ENSDARG00000070081	SPNA1
LSM1	ENSG00000175324	zgc	ENSDARG00000035810	SRI
LSM3	ENSG00000170860	zgc	ENSDARG00000028087	ST3GAL5
LSM4	ENSG00000130520	zgc	ENSDARG00000017710	STX2
LSM5	ENSG00000106355	zgc	ENSDARG00000079964	TBCEL
lsm6	ENSG00000164167	zgc	ENSDARG00000067524	TCEA1
matK	ENSG00000007264	zgc	ENSDARG00000052109	TLR6
MBD2	ENSG00000134046	zgc	ENSDARG00000038794	TMEM56
Mcm10	ENSG00000065328			TMPO
mcm2	ENSG00000073111			TPRGL
MCM3	ENSG00000112118			TSPAN8
MCM4	ENSG00000104738			UBAC1
Mcm5	ENSG00000100297			UBLCP1
MCM6	ENSG00000076003			USP7
Mnat1	ENSG00000020426			XPO7
MPP6	ENSG00000105926			
mre11a	ENSG00000020922			
mRpS12	ENSG00000128626			
Msh2	ENSG00000095002			
msh3	ENSG00000113318			
msh6	ENSG00000116062			
MT1G	ENSG00000125144			
mthfd1	ENSG00000100714			
Mutyh	ENSG00000132781			
myb	ENSG00000118513			
mybbp1a	ENSG00000132382			

MYBL2	ENSG00000101057
MYC	ENSG00000136997
Myst2	ENSG00000136504
NANOG	ENSG00000111704
ncI	ENSG00000115053
NFKBIB	ENSG00000104825
NLE1	ENSG00000073536
Nme1	ENSG00000011052
noc2l	ENSG00000188976
Nop56	ENSG00000101361
NOLA1	ENSG00000109534
NOLC1	ENSG00000166197
NOP58	ENSG00000055044
NP	ENSG00000198805
Npm1	ENSG00000181163
nppb	ENSG00000120937
nthl1	ENSG00000065057
Nudt1	ENSG00000106268
NUP153	ENSG00000124789
NUP50	ENSG00000093000
Orc1l	ENSG00000085840
ORC2L	ENSG00000115942
ORC6L	ENSG00000091651
Otx2	ENSG00000165588
PA2G4	ENSG00000170515
Pak1	ENSG00000149269
Pak3	ENSG00000077264
parp1	ENSG00000143799
PASK	ENSG00000115687
PBX1	ENSG00000185630
pcnA	ENSG00000132646
Pcyt1b	ENSG00000102230
pelp1	ENSG00000141456
pfdn6	ENSG00000204220
pfn1	ENSG00000108518
Phb	ENSG00000167085
PHC1	ENSG00000111752
Phf10	ENSG00000130024
PHGDH	ENSG00000092621
PIAS2	ENSG00000078043
plscr1	ENSG00000188313
PMAIP1	ENSG00000141682
pmf1	ENSG00000160783
PNN	ENSG00000100941
Pold1	ENSG00000062822
Pold2	ENSG00000106628
POLG2	ENSG00000136480
POLQ	ENSG00000051341
Poir1c	ENSG00000171453
POLR1D	ENSG00000186184

POP1	ENSG00000104356
pop5	ENSG00000167272
POP7	ENSG00000172336
pou5f1	ENSG00000206454
POU5F1	ENSG00000204531
ppan	ENSG00000130810
Ppap2c	ENSG00000141934
ppiD	ENSG00000171497
PPM1B	ENSG00000138032
prmt5	ENSG00000100462
PRNP	ENSG00000171867
PSIP1	ENSG00000164985
Psma3	ENSG00000100567
Psma6	ENSG00000100902
Psmc11	ENSG00000108671
PSME3	ENSG00000131467
PTMA	ENSG00000187514
PTPN6	ENSG00000111679
PXN	ENSG00000089159
rad51	ENSG00000051180
RAD54L	ENSG00000085999
RAD9A	ENSG00000172613
RASL11B	ENSG00000128045
RBM14	ENSG00000173959
Rbpms	ENSG00000157110
RCHY1	ENSG00000163743
Recql4	ENSG00000160957
RFC2	ENSG00000049541
RFC3	ENSG00000133119
Rfc4	ENSG00000163918
RFC5	ENSG00000111445
RMND5B	ENSG00000145916
RND1	ENSG00000172602
RNMTL1	ENSG00000171861
RPA1	ENSG00000132383
RPA2	ENSG00000117748
Rpa3	ENSG00000106399
RPP40	ENSG00000124787
Ruvbl1	ENSG00000175792
sall4	ENSG00000101115
sephs1	ENSG00000086475
set	ENSG00000119335
SFRS1	ENSG00000136450
SFRS2	ENSG00000161547
SFRS3	ENSG00000112081
SIGLEC12	ENSG00000160296
sip1	ENSG00000092208
sirt1	ENSG00000096717
Slc19a1	ENSG00000173638
Smarcad1	ENSG00000163104

smn2	ENSG00000172062
SMNDC1	ENSG00000119953
snrpa	ENSG00000077312
SNRPB	ENSG00000125835
Snrpc	ENSG00000124562
SNRPD1	ENSG00000167088
SNRPE	ENSG00000182004
SNRPF	ENSG00000139343
SNRPN	ENSG00000214265
SNURF	ENSG00000128739
Socs1	ENSG00000185338
sp1	ENSG00000185591
SPAG5	ENSG00000076382
ssb	ENSG00000138385
stip1	ENSG00000168439
STRBP	ENSG00000165209
STX3	ENSG00000166900
STXBP2	ENSG00000076944
STXBP3	ENSG00000116266
Sumo1	ENSG00000116030
Supt3h	ENSG00000196284
SYNCRIP	ENSG00000135316
TARBP2	ENSG00000139546
tcerg1	ENSG00000113649
TCOF1	ENSG00000070814
TDGF3	ENSG00000163828
Tgif1	ENSG00000177426
tk1	ENSG00000167900
TMPO	ENSG00000120802
TMSB4Y	ENSG00000154620
TNFRSF8	ENSG00000120949
TNNI3	ENSG00000129991
toe1	ENSG00000132773
tp53	ENSG00000141510
Tpx2	ENSG00000088325
TRAIP	ENSG00000183763
TRIM28	ENSG00000130726
Trip13	ENSG00000071539
Ttrap	ENSG00000111802
tuba3c	ENSG00000198033
u2af1	ENSG00000160201
UNC119	ENSG00000109103
ung	ENSG00000076248
Vamp8	ENSG00000118640
Vasp	ENSG00000125753
WDR33	ENSG00000136709
WDR77	ENSG00000116455
Wdr8	ENSG00000116213
wee1	ENSG00000166483
wrn	ENSG00000165392

XRCC5	ENSG00000079246
XTP3TPA	ENSG00000179958
Zfp42	ENSG00000179059
ZNF165	ENSG00000197279
ZNF281	ENSG00000162702
znf593	ENSG00000142684

Gene Set Name [# Genes (K)]	Description	# Genes in overlap (k)	p value	Genes
CAIRO_HEPATOBLASTOMA_CLASSES_UP [611]	Genes up-regulated in robust Cluster 2 (rC2) of hepatoblastoma samples compared to those in the robust Cluster 1 (rC1).	19	$0 e^0$	GART, DDX18, PHB, PPAT, ATIC, CAD, BYSL, WDR12, NLE1, NAT10, FBL, NPM1, ECT2, IMP4, MYBBP1A, PDCD11, WDR46, IMPDH2, KARS
DODD_NASOPHARYNGEAL_CARCINOMA_DN [1375]	Genes down-regulated in nasopharyngeal carcinoma (NPC) compared to the normal tissue.	19	$2.91 e^{-13}$	GART, DDX18, PHB, PPAT, ATIC, CAD, FBL, NPM1, ECT2, UMPS, CTPS, MKI67IP, POLR1B, WDR75, NOC3L, HELLS, PPRC1, LARS, RPL7L1
KRIGE_RESPONSE_TO_TOSEDOSTAT_24HR_DN [1022]	Genes down-regulated in HL-60 cells (acute promyelocytic leukemia, APL) after treatment with the aminopeptidase inhibitor tosedostat (CHR-2797) for 24 h.	16	$6.54 e^{-12}$	GART, DDX18, PHB, BYSL, FBL, IMP4, MYBBP1A, PDCD11, WDR46, UMPS, MKI67IP, POLR1B, WDR75, NOC3L, PPAN, NOC4L
WEI_MYCN_TARGETS_WITH_E_BOX [797]	Genes whose promoters contain E-box motifs and whose expression changed in MYCN-3 cells (neuroblastoma) upon induction of MYCN	14	$4.3 e^{-11}$	DDX18, PHB, PPAT, BYSL, WDR12, IMP4, UMPS, CTPS, MKI67IP, POLR1B, WDR75, HELS, PPRC1, SHMT1
BILD_MYC_ONCOGENIC_SIGNATURE [206]	Genes selected in supervised analyses to discriminate cells expressing c-Myc [Gene ID=4609] from control cells expressing GFP.	8	$2.57 e^{-9}$	DDX18, PHB, ATIC, WDR12, NLE1, NPM1, IMP4, MYBBP1A
DANG_MYC_TARGETS_UP [130]	Genes up-regulated by MYC [Gene ID=4609] and whose promoters are bound by MYC, according to MYC Target Gene Database.	7	$2.9 e^{-9}$	DDX18, PHB, PPAT, CAD, NPM1, SHMT1, PRDX3
RHEIN_ALL_GLUCCORTICOID_THERAPY_DN [366]	Genes down-regulated in ALL (acute lymphoblastic leukemia) blasts after 1 week of treatment with glucocorticoids.	9	$1.26 e^{-8}$	ATIC, FBL, NPM1, ECT2, IMPDH2, PRDX3, CNBP, PCCA, PCCB
KINSEY_TARGETS_OF_EWSR1_FLI1_FUSION_UP [1281]	Genes up-regulated in TC71 and EWS502 cells (Ewing's sarcoma) upon knockdown of the EWSR1-FLI1 fusion [Gene ID=2130, 2314].	14	$2 e^{-8}$	GART, DDX18, PPAT, NPM1, ECT2, MYBBP1A, UMPS, CTPS, MKI67IP, NOC3L, HELLS, LARS, SHMT1, PRDX3
MARZEC_IL2_SIGNALING_UP [107]	Genes up-regulated by IL2 [Gene ID=3558] in cells derived from CD4+ [Gene ID=920] cutaneous T-cell	6	$3.37 e^{-8}$	GART, PPAT, PDCD11, UMPS, CTPS, POLR1B

	lymphoma (CTCL).			
PUJANA_BRCA1_PCC_NETWORK [1671]	Genes constituting the BRCA1-PCC network of transcripts whose expression positively correlated (Pearson correlation coefficient, $PCC \geq 0.4$) with that of BRCA1 [Gene ID=672] across a compendium of normal tissues.	15	7.33×10^{-8}	GART, DDX18, ATIC, CAD, BYSL, FBL, NPM1, IMP4, IMPDH2, KARS, CTPS, PRDX3, CNBP, PCCB, METAP1
WELCSH_BRCA1_TARGETS_1_DN [125]	Upregulated by induction of exogenous BRCA1 in EcR-293 cells	6	8.55×10^{-8}	PPAT, ATIC, CAD, BYSL, PDCD11, CTPS
RODRIGUES_THYROID_CARCINOMA_POORLY_DIFFERENTIATED_UP [640]	Genes up-regulated in poorly differentiated thyroid carcinoma (PDTC) compared to normal thyroid tissue.	10	1.26×10^{-7}	GART, PPAT, ATIC, WDR12, NPM1, ECT2, CTPS, MKI67IP, WDR75, HELLS
KRIGE_RESPONSE_TO_TOSEDOSTAT_6HR_DN [920]	Genes down-regulated in HL-60 cells (acute promyelocytic leukemia, APL) after treatment with the aminopeptidase inhibitor tosedostat (CHR-2797) for 6 h.	11	3.9×10^{-7}	GART, DDX18, PHB, IMP4, MYBBP1A, PDCD11, WDR46, UMPS, MKI67IP, POLR1B, PPAN

Mutant Phenotype								
Gene	Mutant	CNSn	MHB	HE	PO	LG	IHV	RY
<i>bysl</i>	<i>bysl</i> ^{hi3351Tg}	x	x	x	x	x	x	x
<i>cad</i>	<i>cad</i> ^{a52} , <i>cad</i> ^{hi2694Tg}			x	x	x		x
<i>ddx18</i>	<i>ddx18</i> ^{hi1727Tg}	x	x	x		x	x	
<i>ect2</i>	<i>ect2</i> ^{hi3820aTg}	x	x					x
<i>fbl</i>	<i>fbl</i> ^{hi2581Tg} ; <i>fbl</i> ^{hi3580Tg}	x	x	x		x	x	x
<i>gart</i>	<i>gart</i> ^{hi3526bTg}							
<i>kars</i>	<i>kars</i> ^{hi2586Tg}			x	x	x		
<i>mki67ip</i>	<i>mki67ip</i> ^{hi1581Tg}							
	<i>mki67ip</i> ^{hi2827bTg}	x					x	
	<i>mki67ip</i> ^{hi4003aTg}							
<i>mybbp1a</i>	<i>mybbp1a</i> ^{hi1552Tg}	x		x	x	x		x
<i>noc3l</i>	<i>noc3l</i> ^{hi1019Tg}							
	<i>noc3l</i> ^{hi3783Tg}	x		x	x	x		x
<i>nop56</i>	<i>nop56</i> ^{hi3101Tg}	x	x	x	x		x	x
<i>nop58</i>	<i>nop58</i> ^{hi3118Tg}	x		x	x	x	x	x
<i>pes</i>	<i>pes</i> ^{hi2Tg}			x		x		
<i>rpl7l1</i>	<i>rpl7l1</i> ^{hi1793Tg}			x	x			
<i>rrp1</i>	<i>rrp1</i> ^{hi2689Tg}							
	<i>rrp1</i> ^{hi2705aTg}			x	x	x	x	x
<i>wdr12</i>	<i>wdr12</i> ^{hi3120Tg}			x	x	x		
<i>wdr46</i>	<i>wdr46</i> ^{hi1451Tg}	x	x	x	x	x	x	x
<i>wdr75</i>	<i>wdr75</i> ^{hi2404Tg}		x	x		x	x	

CNS: Central Nervous System necrosis

MHB: Pinched MHB

HE: Smaller head eyes

PE: pericardial edema

LG: underdeveloped liver/gut

IHV: Inflated hindbrain ventricle

RY: Round grey (unconsumed) yolk

<i>ect2</i>	ENSDARG00000007278	Fwd Rev	CCCTGTCCCAGATCAGAAGA ATTAAATTCGCCCAGACGTG
<i>pes</i>	ENSDARG00000018902	Fwd Rev	TGGGCGGATTACAAAAGAAG GCGGGTAGACAAGGTTGAGA
<i>nop56</i>	ENSDARG0000001282	Fwd Rev	TGGTCAAAGTCTGAGTGCCTTC ACCAATGAGAGCTGCGAGAT
<i>cad</i>	ENSDARG00000041895	Fwd Rev	CTTCATCGCCCCAATACAGT ACGCCCTTCTGGACATCTTT
<i>pcna</i>	ENSDARG00000054155	Fwd Rev	GGCAACATCAAGCTCTCACA TTAAGGGTTGACTGGATGAA